Conformational shifts in a chemoreceptor helical hairpin control kinase signaling in *Escherichia coli*

Qun Gao (高群)[a,b], Anchun Cheng (程安春)[a,1], and John S. Parkinson[b,1]

[a]Institute of Preventive Veterinary Medicine, College of Veterinary Medicine, Sichuan Agricultural University, Chengdu 611130, China; and [b]School of Biological Sciences, University of Utah, Salt Lake City, UT 84112

Edited by Bonnie L. Bassler, Princeton University and Howard Hughes Medical Institute, Princeton, NJ, and approved June 24, 2019 (received for review February 12, 2019)

Motile *Escherichia coli* cells use chemoreceptor signaling arrays to track chemical gradients with exquisite precision. Highly conserved residues in the cytoplasmic hairpin tip of chemoreceptor molecules promote assembly of trimer-based signaling complexes and modulate the activity of their CheA kinase partners. To explore hairpin tip output states in the serine receptor Tsr, we characterized the signaling consequences of amino acid replacements at the salt-bridge residue pair E385-R388. All mutant receptors assembled trimers and signaling complexes, but most failed to support serine chemotaxis in soft agar assays. Small side-chain replacements at either residue produced OFF- or ON-shifted outputs that responded to serine stimuli in wild-type fashion, suggesting that these receptors, like the wild-type, operate as two-state signaling devices. Larger aliphatic or aromatic side chains caused slow or partial kinase control responses that proved dependent on the connections between core signaling units that promote array cooperativity. In a mutant lacking one of two key adapter-kinase contacts (interface 2), those mutant receptors exhibited more wild-type behaviors. Lastly, mutant receptors with charged amino acid replacements assembled signaling complexes that were locked in kinase-ON (E385K|R) or kinase-OFF (R388D|E) output. The hairpin tips of mutant receptors with these more aberrant signaling properties probably have nonnative structures or dynamic behaviors. Our results suggest that chemoeffector stimuli and adaptational modifications influence the cooperative connections between core signaling units. This array remodeling process may involve activity-dependent changes in the relative strengths of interface 1 and 2 interactions between the CheW and CheA.P5 components of receptor core signaling complexes.

chemotaxis | receptor array | core complex | in vivo FRET

Motile bacteria can detect and track chemical gradients, a behavior known as chemotaxis. The molecular machinery of bacterial chemotaxis comprises a highly organized network of transmembrane chemoreceptors that control a histidine kinase signaling partner. With relatively few components, yet sophisticated signaling properties, bacterial chemotaxis offers a powerful experimental system for exploring mechanisms of transmembrane and intracellular signaling in molecular detail. In this regard, the extensively studied *Escherichia coli* chemotaxis model is arguably the best understood of all biological signal transduction systems (1, 2).

The two principal chemoreceptors of *E. coli*, Tar (aspartate and maltose sensing) and Tsr (serine and AI-2 sensing), are members of a superfamily of bacterial and archaeal proteins known as methyl-accepting chemotaxis proteins (MCPs) (3). Tar and Tsr are homodimeric molecules of ~550-residue subunits with a common functional architecture (Fig. 1*A*): A ligand-binding domain external to the cytoplasmic membrane senses chemoeffectors and conveys stimulus signals through transmembrane helices to a HAMP domain on the cytoplasmic side of the membrane. The four-helix HAMP bundle (4) in turn modulates the conformation of an extended, antiparallel four-helix coiled coil (5) containing sites for sensory adaptation. Sensory inputs culminate at a kinase control domain at the membrane-distal hairpin tip that transmits signals to the cell's rotary flagellar motors. Two hairpin tip residues of Tsr, E385 and R388, are subjects of the present study.

Receptors of different detection specificities can form mixed trimers of dimers through interactions between their highly conserved cytoplasmic hairpin tips (6, 7) (Fig. 1*B*). Receptor core complexes, the fundamental signaling unit, contain two receptor trimers of dimers, one homodimeric, multidomain histidine autokinase (CheA) and two molecules of a scaffolding protein (CheW) (8–10). CheW couples CheA autophosphorylation activity to receptor control through interaction with the CheA.P5 domain at interface 1 (Fig. 1*C*). CheA phosphoryl groups serve, in turn, as phosphodonors for the CheY response regulator, an aspartate autokinase. The phosphorylated form of CheY (P-CheY) binds to the flagellar rotational switch to trigger clockwise reversals that initiate random changes in swimming direction (11). Attractant stimuli down-regulate CheA, thereby augmenting counterclockwise flagellar rotation, the default behavior that produces forward swimming movements.

The signaling properties of receptor core units approximate two-state behavior (12). Both chemoeffector stimuli and covalent adaptational modifications shift an equilibrium between kinase-active (ON) and kinase-inactive (OFF) signaling complexes to control locomotor behavior. Attractant ligands initiate behavioral responses by reducing the kinase activity of receptor complexes. These signaling changes in turn trigger a slower sensory adaptation process that works to restore prestimulus kinase activity, thereby enabling the cell to detect and respond to

Significance

Motile bacteria use chemoreceptor signaling arrays to track chemical gradients with high precision. The *Escherichia coli* chemotaxis system offers an ideal model for probing the molecular mechanisms of transmembrane and intracellular signaling. In this study, we characterized the signaling properties of mutant *E. coli* receptors that had amino acid replacements in residues that form a salt-bridge connection between the cytoplasmic tips of receptor molecules. The mutant signaling defects suggested that the chemoreceptor tip operates as a two-state device with discrete active and inactive conformations and that the level of output activity modulates connections between receptor signaling units that produce highly cooperative responses to attractant stimuli. These findings shed important light on the nature and control of receptor signaling states.

Author contributions: Q.G. and J.S.P. designed research; Q.G. performed research; Q.G., A.C., and J.S.P. analyzed data; and Q.G., A.C., and J.S.P. wrote the paper.

The authors declare no conflict of interest.

This article is a PNAS Direct Submission.

[1]To whom correspondence may be addressed. Email: chenganchun@vip.163.com or parkinson@biology.utah.edu.

This article contains supporting information online at www.pnas.org/lookup/suppl/doi:10.1073/pnas.1902521116/-/DCSupplemental.

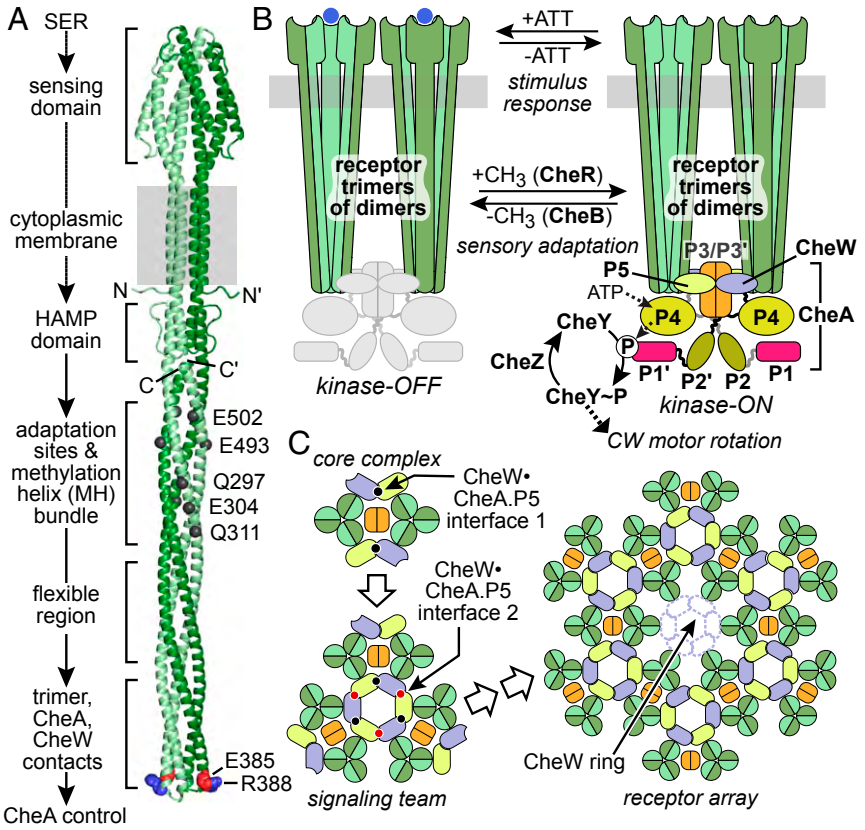

Fig. 1. Chemoreceptor signaling architecture. (*A*) Tsr dimer. Atomic coordinates for an MD-modeled Tsr homodimer were provided by Keith Cassidy; flexible linkers at the C terminus of each subunit are omitted. Spheres show atoms of residues important to the present work, scaled at 1.5× their van der Waals radii for emphasis. Black spheres depict α-carbons at the five modification sites in each subunit; side-chain atoms of residue E385 (red) and residue R388 (blue) lie at the helical hairpin tip. (*B*) Signaling states of the receptor core complex. Attractants (blue spheres) and adaptational modifications promoted by the cytoplasmic CheR and CheB enzymes shift signaling complexes between kinase-active (ON) and kinase-inactive (OFF) outputs. The CheA homodimer contains five domains (P1-P5; P1′-P5′) in each subunit. (*C*) Organization of receptor arrays. The core complex cartoon depicts a top-down cross-section view through the hairpin tip region at the P5-CheW plane. The color scheme corresponds to that of the kinase-ON complex in *B*. Semicircles indicate the inner (light green) and outer (dark green) subunits of each receptor dimer. Core units assemble through CheW-CheA.P5 interface 2 interactions to form cooperative signaling teams. The extended array also contains hexameric CheW rings (9, 18).

subsequent attractant increases as it swims about in chemoeffector gradients. Sensory adaptation involves methylation and demethylation of specific glutamic acid residues interposed between the HAMP domain and hairpin tip of the receptor cytoplasmic domain. Methylation, catalyzed by CheR, enhances receptor kinase activity; demethylation, catalyzed by CheB, reduces kinase activity. The signaling state of the methylation helices regulates their substrate properties for the adaptation enzymes. OFF-shifted receptors are preferred substrates for CheR; ON-shifted receptors are preferred substrates for CheB (13–15).

Chemoreceptor core units assemble into large arrays through a second CheW–CheA.P5 interaction surface at interface 2 (Fig. 1*C*). Interface 2 connections between core units form signaling teams linked by hexagonal CheW-P5 rings that form higher-order hexagonal arrays through additional interface 2 links (Fig. 1*C*). Interface 2 connections enable the receptor array to operate as a multisubunit allosteric enzyme that produces highly cooperative kinase control responses (16, 17).

Although the overall architecture of receptor arrays has been established (9, 10, 18), array operation at the molecular level remains poorly understood. In particular, it is not yet clear how receptor core units function to activate and regulate the CheA kinase. What are the key conformational or dynamic differences between ON-state and OFF-state receptors? How do those receptor structures control CheA activity? How do CheA activity changes propagate through the networked signaling teams in an array? How do adaptational modifications regulate these events? We investigated these issues by examining the signaling roles of two highly conserved residues, E385 and R388, near the helical hairpin tip of the Tsr receptor (Fig. 1*A*). In a crystal structure of the Tsr trimer of dimers (5), the E385-R388 residues occupy two distinct locations: those in the inner dimer subunits lie at the trimer axis; those in the outer subunits lie at the trimer periphery. In the outer subunit location, E385 and R388 lie adjacent to receptor residues that contact CheW and CheA.P5 in core signaling complexes (9, 10, 19). In the inner subunit location, E385 and R388 form interdimer salt bridges that might make important contributions to trimer stability, although most trimer contact residues lie a bit further from the tip (5). In both subunit locations, E385 and R388 occupy the helix-packing layer nearest the hairpin bend of the tip (Fig. 1*A*), just below F396 residues whose stacking arrangement has been suggested to modulate conformational switching at the tip (20).

Our mutational analyses of E385 and R388 revealed that these Tsr residues are not critical for trimer or core complex assembly, but rather stabilize alternative tip conformations whose interplay controls kinase activity and stimulus response. Nearly all amino acid replacements at either residue abrogated chemotaxis due to defects in CheA control, array cooperativity, or sensory adaptation. These findings shed important light on the nature and control of receptor signaling states and suggest refined working models that make testable mechanistic predictions.

Results

Tsr-E385 and Tsr-R388 Mutants. We constructed a complete set of amino acid replacements at Tsr residue E385 by all-codon mutagenesis (21) in plasmid pPA114, which expresses the *tsr* gene under tight salicylate-inducible control (6). Twelve of the mutant receptors (hereafter designated E385*) promoted some serine chemotaxis in UU2612, a receptorless but adaptation-competent strain ($CheR^+$ $CheB^+$; hereafter R+B+). Seven E385* receptors failed to support serine chemotaxis in soft-agar assays (*SI Appendix*, Fig. S1). All mutant receptors expressed at or near native level (*SI Appendix*, Table S2), indicating that their chemotaxis phenotypes reflect functional changes in the mutant proteins rather than folding or stability defects.

In a prior study (22), a complete set of amino acid replacements at Tsr residue R388, the salt-bridge partner of E385 (Fig. 1), was constructed and initially characterized in isopropyl β-D-thio-galactopyranoside (IPTG)-inducible Tsr expression plasmid pCS53 (23). Those mutant receptors (hereafter designated R388*) all exhibited normal intracellular levels, implying near-native

structure, but most failed to support serine chemotaxis in soft agar assays. Tsr proteins encoded by pCS53 and its mutant derivatives carry the S366C reporter site for directly assessing receptor trimer-of-dimer formation with in vivo cross-linking assays (7). None of the R388* receptors proved defective in trimer formation, indicating that the E385–R388 salt bridge interaction is not critical for trimer assembly or stability (22). To better compare the signaling properties of R388* receptors to those of E385* receptors, we chose representative R388* side-chain classes and restored the wild-type serine at residue 366 in the mutant receptors. Those R388* chemotaxis phenotypes are summarized in *SI Appendix*, Fig. S1.

Signaling Properties of E385* and R388* Receptors. We assessed the signaling properties of mutant receptors with an in vivo Förster resonance energy transfer (FRET) kinase assay that monitors the phosphorylation-dependent interaction of phospho-CheY with its phosphatase partner CheZ, using CheZ-CFP (FRET donor) and CheY-YFP (FRET acceptor) fusion proteins (24, 25). Under steady-state conditions, autophosphorylation of CheA is the rate-limiting step in CheY phosphorylation, so the FRET signal (YFP/CFP emissions) provides a readout of cellular CheA activity and its response to chemoattractant stimuli. This FRET assay yields three signaling parameters: (*i*) the response $K_{1/2}$, a measure of receptor sensitivity; (*ii*) the Hill coefficient, reflecting response cooperativity; and (*iii*) the maximal level of kinase activity in the absence of attractant stimuli relative to that of cells with wild-type receptor signaling complexes.

We measured FRET behaviors in two host strains carrying mutant receptor plasmids induced to native Tsr expression levels. In UU2567, a host lacking the sensory adaptation enzymes ($CheR^-$ $CheB^-$; hereafter R−B−), Tsr molecules retain a QEQEE residue pattern at the five adaptation sites in each subunit (Fig. 1). Unmodified methyl-accepting glutamyl (E) residues have OFF-shifting output effects; glutaminyl (Q) residues mimic the ON-shifting effects of methylated (Em) sites (26, 27). In the UU2567 host, wild-type Tsr molecules in the QEQEE modification state exhibit intermediate kinase-activity and serine sensitivity. In UU2700, a host that has the sensory adaptation enzymes (R+B+), wild-type Tsr molecules undergo irreversible CheB-mediated Q to E deamidation reactions and reversible CheR-mediated methylation and CheB-mediated demethylation reactions at the adaptation sites, culminating in a heterogeneous receptor population with a low average modification state and typically more OFF-shifted output than that of QEQEE receptors.

The signaling properties of E385* and R388* receptors are summarized by residue and side-chain class in *SI Appendix*, Fig. S2 and by their signaling defects in Fig. 2. Most of the mutant receptors showed different kinase activities and serine-response behaviors in the adaptation-deficient and adaptation-proficient hosts, indicating that their mutant outputs were amenable to some sensory adaptation control. To assess their substrate properties

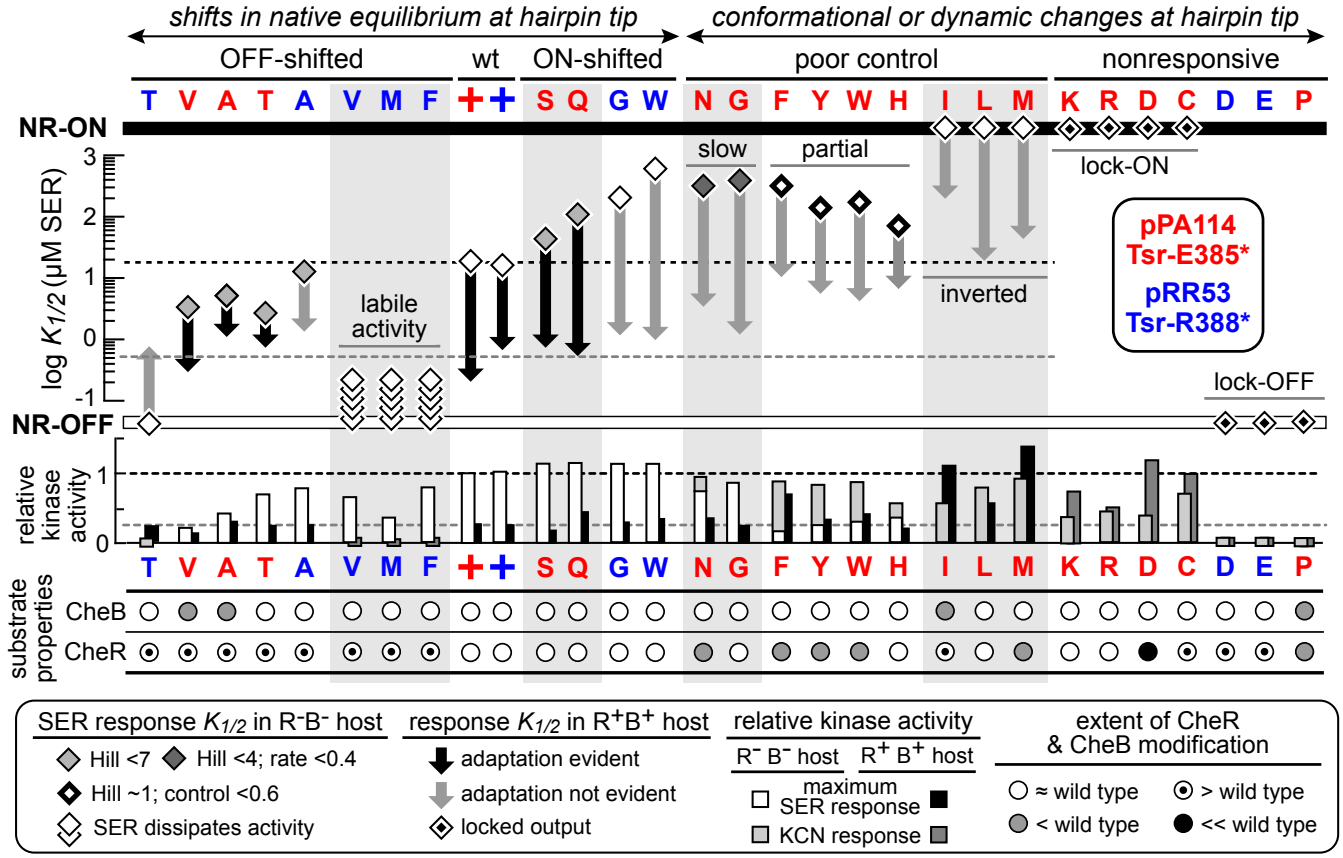

Fig. 2. Signaling properties of Tsr-E385* and Tsr-R388* receptors. Amino acid replacements in mutant receptors, grouped by signaling class, are indicated with one-letter designations; +, wild-type residue. Red letters indicate E385* mutants; blue letters indicate R388* mutants. *Top* and *Middle* summarize data from FRET kinase assays. Dashed horizontal lines indicate $K_{1/2}$ values for wild-type Tsr in the UU2567 (R−B−; black line) and UU2700 (R+B+; gray line) hosts. In our laboratory, SDs for $K_{1/2}$ measurements are typically less than ±25%; those for Hill coefficients and kinase activities are typically less than ±50% (16, 26, 46, 71, 78–81). The two wild-type plasmids (pPA114 and pRR53) produced slightly different $K_{1/2}$ values in UU2700; so the dashed gray line is at the average of those two values. All kinase activities are normalized to that of wild-type Tsr in UU2567 and represent the larger of the activity inhibited by a saturating serine stimulus (white and black bars) or by KCN treatment (light gray and dark gray bars). *Bottom* summarizes the extent of receptor modification by the CheR and CheB adaptation enzymes, as defined in *Materials and Methods*.

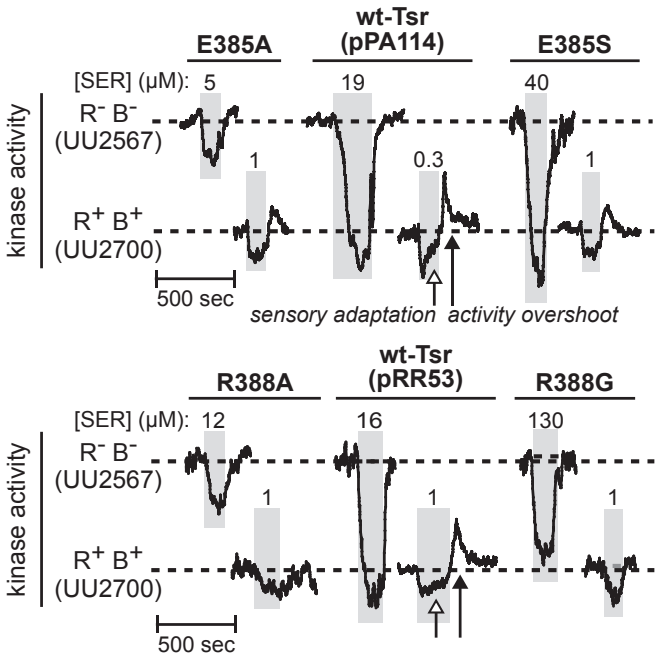

Fig. 3. Examples of output-shifted E385* and R388* receptors. Kinase responses are shown as changes in the prestimulus ratio of CheY-YFP to CheZ-CFP emission counts in FRET kinase assays. Dashed lines indicate relative baseline activities in adaptation-deficient (UU2567) and adaptation-proficient (UU2700) hosts. All traces have the same activity and time scales. Gray rectangles indicate periods during which cells experienced the indicated concentrations of serine. Serine stimuli were at or near the $K_{1/2}$ concentrations. In the adaptation-competent host, wild-type Tsr shows relatively rapid recovery of kinase activity (open arrow) after the serine stimulus, followed by a spike in kinase activity (filled arrow) upon serine removal due to an increase in receptor methylation during the adaptation phase. The spike in kinase activity rapidly returns to the prestimulus baseline through CheB-mediated demethylation reactions.

for the sensory adaptation enzymes, we expressed the mutant receptors in hosts containing either CheR or CheB and examined their electrophoretic migration patterns in denaturing polyacrylamide gels, which can distinguish receptors in different modification states (28–30) (*SI Appendix*, Fig. S2). In single-enzyme hosts, OFF-shifted receptors should be more readily modified by CheR than by CheB, whereas ON-shifted receptors should be more readily modified by CheB than by CheR.

The signaling and adaptational substrate properties of E385* and R388* receptors defined two general structure-function classes (Fig. 2): Mutants whose principal signaling change is an altered response threshold ("OFF-shifted"; "ON-shifted"; Fig. 2) may represent equilibrium shifts between native ON and OFF tip conformations. Mutant receptors with aberrant or no output control ("poor control" and "nonresponsive" in Fig. 2) probably have more drastic changes in tip structure or stability. These general signaling classes are described in more detail below.

Mutant Receptors with OFF-Shifted or ON-Shifted Outputs. The E385A|V|T and R388A|V|T|M|F receptors exhibited OFF-shifted behaviors characterized by extensive CheR modification and reduced kinase activity and/or serine response threshold (Fig. 2). The E385S|G and R388G|W receptors exhibited ON-shifted behaviors, characterized by full kinase activities, elevated $K_{1/2}$ serine responses, and wild-type extents of modification by both CheB and CheR (Fig. 2). The amino acid replacements in these output-shifted receptors may alter the relative stabilities of the native tip structures to shift an equilibrium between kinase-ON and kinase-OFF signaling conformations.

The signaling properties of output-shifted E385* and R388* receptors differed in several respects (Fig. 2). In the adaptation-deficient host, OFF-shifted receptors at both residues had substantially reduced response cooperativities (*SI Appendix*, Table S2). However, the ON-shifted E385*S|Q receptors also had low response cooperativities, whereas the ON-shifted R388G|W receptors had wild-type Hill coefficients (*SI Appendix*, Table S3). In the adaptation-competent host, all output-shifted E385* mutants showed clear evidence of sensory adaptation (E385A|S in Fig. 3; E385V|T|Q in *SI Appendix*, Fig. S3), whereas adaptation to a $K_{1/2}$ serine stimulus was less apparent in the output-shifted R388* mutants (R388A|G in Fig. 3; R388T|W in *SI Appendix*, Fig. S3). Both groups of receptors exhibited essentially wild-type steady-state kinase activities in the R+B+ host, indicating that the mutant receptors are capable of achieving adaptational output control, albeit more slowly than wild-type Tsr. Among all R388* mutants, only the R388K receptor exhibited adaptation behavior similar to the wild type. However, its kinase activity was notably higher in the adaptation-proficient host than in the adaptation-deficient host (*SI Appendix*, Figs. S2 and S3), a behavior we address in *Discussion*.

The more severely OFF-shifted R388V|M|F receptors produced some kinase activity in the R−B− host but failed to fully recover that activity following a serine stimulus (Fig. 4). In the R+B+ host, these receptors produced no appreciable kinase activity (Figs. 2 and 4); Attractant stimuli and the sensory adaptation system seem to regulate not only the kinase activities of wild-type receptors but also the average size of signaling teams in the receptor array (16, 17, 31–33). Kinase-ON output favors large teams; kinase-OFF output favors smaller teams. To ask whether changes in signal team size might play a role in kinase lability behaviors, we examined the R388V|M|F receptors in adaptation-deficient strain UU2869, which has a mutant CheW (W-X3) incapable of forming array interface 2 connections between core units (16). Wild-type Tsr retained near-normal kinase activity in UU2869 but responded to serine with enhanced sensitivity and greatly reduced cooperativity, hallmarks of non-networked signaling teams (*SI Appendix*, Fig. S3 *D* and *E*). The R388V|M|F receptors, however, produced no kinase activity in UU2869 (Fig. 4 and *SI Appendix*, Table S4). We conclude that the side-chain replacements in these mutant receptors destabilize the kinase-ON state but may also serve to trap the receptor in a kinase-OFF state after responding to a serine pulse.

Mutant Receptors with Poor Output Control. In the adaptation-deficient host, the E385G and E385N receptors produced

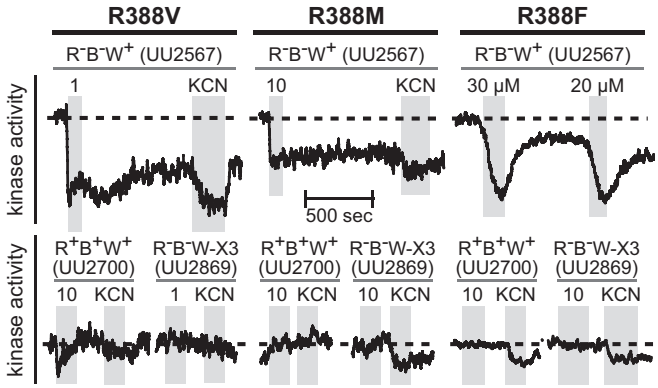

Fig. 4. OFF-shifted R388* receptors with labile kinase activities. Kinase responses are shown as changes in the prestimulus ratio of CheY-YFP to CheZ-CFP emission counts in FRET kinase assays. Dashed lines indicate only prestimulus baselines, not activity levels relative to other hosts. However, all traces have the same activity and time scales. Gray rectangles indicate periods during which cells experienced the indicated concentrations of serine. Serine stimuli were at saturating concentrations for all but R388F in the UU2567 host.

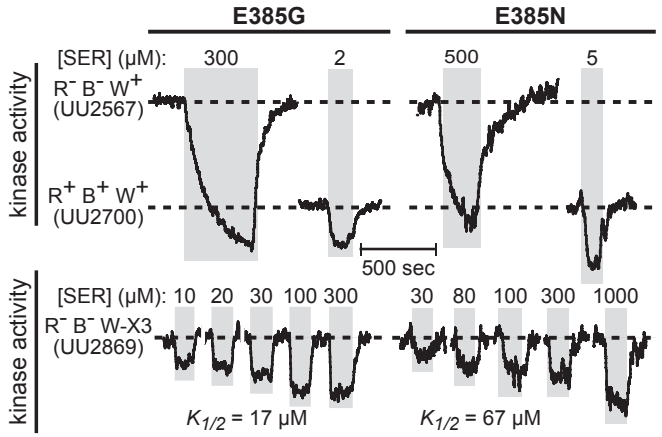

Fig. 5. E385* receptors with slow kinase-control responses. Kinase responses are shown as changes in the prestimulus ratio of CheY-YFP to CheZ-CFP emission counts in FRET kinase assays. Dashed lines in *Upper* indicate relative kinase activities in the UU2567 and UU2700 hosts but are not related to the activity baseline for the UU2869 host. However, all traces have the same activity and time scales. Gray rectangles indicate periods during which cells experienced the indicated concentrations of serine. Serine stimuli are at $K_{1/2}$ concentrations in *Upper*.

notably slow, low-cooperativity kinase-inhibition responses to a $K_{1/2}$ serine stimulus; recovery of kinase activity upon serine removal was also slow (Fig. 5). However, their stimulus responses were not especially slow in the adaptation-competent host (Fig. 5), suggesting that adaptational adjustments of output activity or array connectivity might accelerate their response kinetics. Array connectivity is most likely the critical factor because the mutant responses also exhibited wild-type kinetics in the CheW-X3 host (Fig. 5 and *SI Appendix*, Table S4).

The E385F|Y|W|H receptors exhibited noncooperative, partial kinase-control responses in the adaptation-deficient host (E385Y in Fig. 6; E385F|W|H in *SI Appendix*, Fig. S4 *A–C*). These mutant receptors produced near-normal levels of kinase activity but down-regulated less than half of that activity in response to a saturating serine stimulus. An adaptation-competent host remedied this aberrant behavior (Fig. 6 and *SI Appendix*, Fig. S4 *A* and *B*), implying that its origins might be mechanistically related to those of the slow-response receptors. Indeed, the CheW-X3 host also alleviated partial control of kinase activity by this group of receptor mutants (e.g., E385Y in Fig. 6 and *SI Appendix*, Table S4), indicating that network connections between core signaling units impair their signaling behaviors.

The partial responses of E385F|Y|W|H receptors in the host lacking sensory adaptation enzymes resembled in several respects those of wild-type Tsr in an adaptation-proficient host (compare Figs. 3 and 6). The E385Y (Fig. 6) and E385W (*SI Appendix*, Fig. S4*B*) responses were especially notable. Serine concentrations near their response $K_{1/2}$ elicited down-regulation of kinase activity, followed by a rapid return of prestimulus activity. Upon serine removal, kinase activity increased briefly, reminiscent of the activity overshoot produced by methylation of the wild-type receptor in an adaptation-competent host. However, in the host containing CheR and CheB, the E385Y and E385W receptors showed no adaptation behaviors (Fig. 6 and *SI Appendix*, Fig. S4*B*), suggesting that the QEQEE modification state is important to their kinase recovery process. In the CheW-X3 host, the E385Y receptor showed complete control of kinase activity and no adaptation-like behavioral responses (Fig. 6); in contrast, the E385W receptor lost all kinase activity (*SI Appendix*, Fig. S4*B*). We conclude that network connections between the core signaling complexes of these mutant receptors play important roles not only in producing their kinase activities but also in implementing their adaptation-like behaviors in the absence of the CheR and CheB enzymes.

The E385I|L|M receptors produced kinase activity in the R−B− host but failed to respond to even very high concentrations of serine (Fig. 2). Although they responded to serine in the R+B+ host, those signaling behaviors were unusual in several respects: For example, both the E385I receptor, a superb CheR substrate, and E385M, a poor CheR substrate, showed very high kinase activities in the R+B+ host, despite gaining the ability to down-regulate that activity in response to serine (Fig. 2 and *SI Appendix*, Fig. S3*B*). The serine response of the E385I receptor also exhibited slow kinetics consistent with concomitant array remodeling events (*SI Appendix*, Fig. S3*B*). We designate these mutant receptors as "inverted" because the sensory adaptation system increased their kinase activities. In *Discussion*, we suggest a mechanism for this behavior.

Mutant Receptors with Locked Outputs. The R388D|E and E385P receptors produced no kinase activity in either R−B− or R+B+ FRET hosts (Fig. 2 and *SI Appendix*, Tables S2 and S3). In principle, these locked-OFF outputs might simply reflect an inability to assemble signaling complexes. However, these mutant receptors did form cellular clusters in strain UU3406, which expresses a CheA::mYFP reporter (*SI Appendix*, Fig. S5*A*). Over 85% of UU3046 cells containing wild-type Tsr receptors exhibited one or several fluorescent spots; the locked-OFF E385P and R388D receptors (and the severely OFF-shifted R388T receptor) produced fluorescent spots similar to the wild-type in size and location, albeit at somewhat lower frequency (*SI Appendix*, Fig. S5*A*). The R388E receptor actually produced more prominent and more numerous clusters than the wild-type control (*SI Appendix*, Fig. S5*A*). Thus, the kinase-OFF outputs of these mutant receptors are not due to failure to assemble core signaling complexes. The R388D|E receptors were highly modified by CheR, consistent with a native OFF-output state. In contrast, the E385P receptor appears to have a nonnative tip structure. It was a very poor

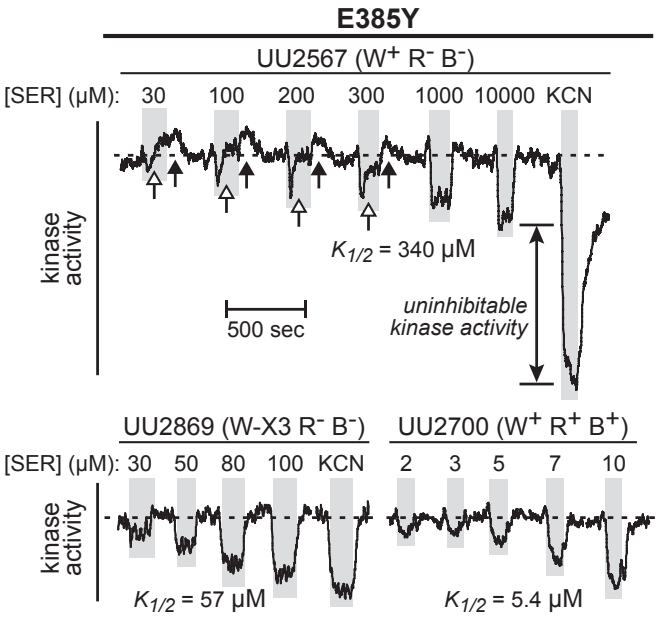

Fig. 6. Kinase control responses of the E385Y receptor. Kinase activity responses are shown as changes in the prestimulus ratio of CheY-YFP to CheZ-CFP emission counts in FRET kinase assays. All traces have the same activity and time scales. Gray rectangles indicate periods during which cells experienced the indicated concentrations of serine. Arrows indicate adaptation-like behaviors in the UU2567 host, which lacks sensory adaptation enzymes. The derived $K_{1/2}$ concentrations are shown below the traces; other parameter values are given in *SI Appendix*, Fig. S5.

substrate for CheR and CheB modifications (Fig. 2), suggesting that its methylation helix bundle lies outside the preferred substrate conformation for either adaptation enzyme.

The E385K|R|D|C receptors produced serine-impervious kinase activity in both FRET tester hosts (Fig. 2). Similar to the inverted E385I|L|M mutants, these locked-ON receptors exhibited high kinase activity in the adaptation-competent host and disparate substrate properties for the adaptation enzymes: E385D was refractory to CheR modification, E385C was extensively modified by CheR, and E385K|R were modified to wild-type extent by both CheR and CheB (Fig. 2).

The signaling properties of the E385K|R and R388D|E receptors were more extreme than those produced by uncharged amino acid replacements (Fig. 2). Their locked outputs might reflect substantial destabilization of local structure due to charge repulsion between the wild-type side chain at one residue and a charge-reversed side chain at the other. If so, then doubly mutant receptors with charge reversals at both residues might have more normal signaling properties. This proved to be the case: In the adaptation-proficient strain, all four doubly mutant receptors produced appropriately adjusted levels of kinase activity and down-regulated that activity in response to serine (*SI Appendix*, Fig. S5*B*). However, the doubly mutant receptors did not exhibit sensory adaptation and did not support serine chemotaxis in soft agar tests.

Discussion

CheA Control in Chemoreceptor Signaling Complexes. The autophosphorylation activity of CheA coupled to receptors in core signaling units is more than 100-fold greater than that of CheA molecules alone (34–36). That activity increase is largely due to enhancement of CheA domain interactions that occur rarely in uncoupled molecules (37–40). The short linkers that join the CheA ATP-binding domain (P4) to its flanking dimerization (P3) and CheW-binding (P5) domains play key roles in receptor-coupled activation (39, 41, 42), conceivably by stabilizing the P3/P4 and P4/P5 interfaces (Fig. 1). In kinase-ON signaling complexes, the phospho-accepting CheA.P1 domain is in dynamic motion, presumably reflecting transient interactions with the P4 domain during the autophosphorylation reaction cycle (38, 43). In kinase-OFF complexes, the P1 domain is more static, perhaps stably docked to the P4 domain (43).

In core units, the hairpin tip of one receptor molecule in each trimer contacts the P5 domain of one CheA subunit (Fig. 1) (44, 45), but that interaction is not critical to CheA control (46). Rather, the CheW-bound receptor in each trimer probably controls CheA activity through the CheW-CheA.P5 interface 1 connection (Fig. 1) (46, 47), in turn enabling P5 to control P4 through their mutual interface and connecting linker (41, 42). To mediate CheA control, the tip of the CheW-bound receptor might transmit dynamic motions to P5 or it might propagate discrete conformational changes to P5. In either case, the signaling-related motions appear to be small (47).

Signal Transmission from HAMP to the Hairpin Tip. Signal transmission in the cytoplasmic domains of MCP-family chemoreceptors proceeds mainly through opposed dynamic coupling of adjacent structural elements (2, 48). Attractant stimuli trigger kinase-OFF output by enhancing the packing stability of the HAMP four-helix bundle (49–51), which in turn reduces the stability of the methylation helices (52–54) or their packing interactions in the MH bundle (49, 50, 55, 56). The sensory adaptation system restores prestimulus kinase activity by reversing those MH bundle structural changes (54, 57).

The yin-yang model of output control in chemoreceptors proposed that the MH bundle and hairpin tip might also be coupled in frozen-dynamic opposition through the intervening flexible region and glycine hinge (Fig. 7*A*) (58). The structural coupling mechanism might involve axial rotation of the flexible region helices (56) or opposed helix-packing arrangements above and below the glycine hinge (3). In any case, the glycine hinge residues clearly play an important role in signal transmission to the tip (59, 60). A number of in vitro structural studies support dynamics-based signal transmission in chemoreceptors but have not provided a consensus view of output-dependent differences in dynamic behavior at the hairpin tip (52, 55, 61–63).

All known MCP-family chemoreceptors contain a phenylalanine pair at the center of the protein interaction region in their hairpin tips (3, 20). This invariant structural feature must play a key role in the receptor tip signaling mechanism. An all-atom molecular dynamics (MD) analysis of Tsr (the region shown in Fig. 7*A*) revealed flips in the aromatic stacking arrangement of F396 residues at the subunit interface that accompanied discrete conformational changes in the tip (20) (Fig. 7*C*). One conformation predominated in a Tsr [EEEEE] model with unmodified adaptation sites; the other predominated in a Tsr [QQQQE] model with methyl-mimicking Q residues at four of the five adaptation sites. A Tsr [QEQEE] model switched frequently between these two conformations, spending comparable time in each. Ortega et al. (20) suggested that these alternative tip structures represent kinase-OFF and kinase-ON output states and that aromatic stacking of F396 residues constrains the tip to these two conformations. In this two-state view of tip signaling, the flexible region and glycine hinge would shift the ON-OFF output equilibrium by transmitting helix rotation or bundle-twisting motions that favor one or the other aromatic stacking arrangement. We make the case below that the signaling properties of Tsr-E385* and R388* receptor mutants are best explained by a two-state mechanism for tip signaling.

Experimental Support for a Two-State Model of Hairpin Tip Signaling. The E385 and R388 residues form salt bridge connections between adjacent dimers in the Tsr [QQQQE] trimer crystal structure (5) (Fig. 7*B*), which most likely represents a kinase-ON conformation (5–7, 64). An MD-derived model of the kinase-ON core complex also exhibits the salt-bridge arrangement (18). The salt bridge is not essential for trimer stability or core complex formation because mutant E385* and R388* receptors efficiently assembled core signaling complexes and arrays (this study; ref. 22). It follows that the E385 and R388 residues in the outer subunits of trimers (Fig. 7*B*) also play no critical role in CheW or CheA.P5 interactions. The E385-R388 salt bridge is also not important for CheA activation or control because many of the mutant receptors, including E385G and R388G, promoted wild-type kinase activities and responded to serine stimuli in both adaptation-deficient and adaptation-proficient hosts. Although the glycine replacement receptors had elevated serine response thresholds, seemingly consistent with a dynamic ON-state structure, other side-chain replacements that might be expected to destabilize the native trimer structure (e.g., E385A|P; R388D|E) did not cause ON-shifted outputs.

At its trimer-axis location, the R388 side chain is solvent-exposed and relatively unconstrained, whereas the E385 side chain resides in a cavity, packed against the C′-helix of the other subunit in the receptor dimer (Fig. 7 *B* and *C*). Amino acid replacements at either residue can disrupt the interdimer salt bridges in trimers, but owing to packing constraints, E385* replacements could have more drastic structural and functional consequences than their R388* counterparts. Indeed, small side-chain replacements were relatively well-tolerated at both positions, whereas larger replacements, especially at E385, caused more aberrant signaling properties. The A|V|T replacements at E385 or R388 caused OFF-shifted outputs; other replacements (E385S|Q; R388G|W) produced ON-shifted behaviors. These mutant receptors all responded to serine control in both adaptation-proficient and adaptation-deficient hosts. We conclude that they have only modest changes in structure and function at the hairpin tip. In the context of a two-state tip model, their shifted outputs could be due to a change in the relative stabilities of the native ON and OFF conformations.

Other side-chain replacements produced more drastic signaling defects: slow response kinetics (E385N|G); partial kinase

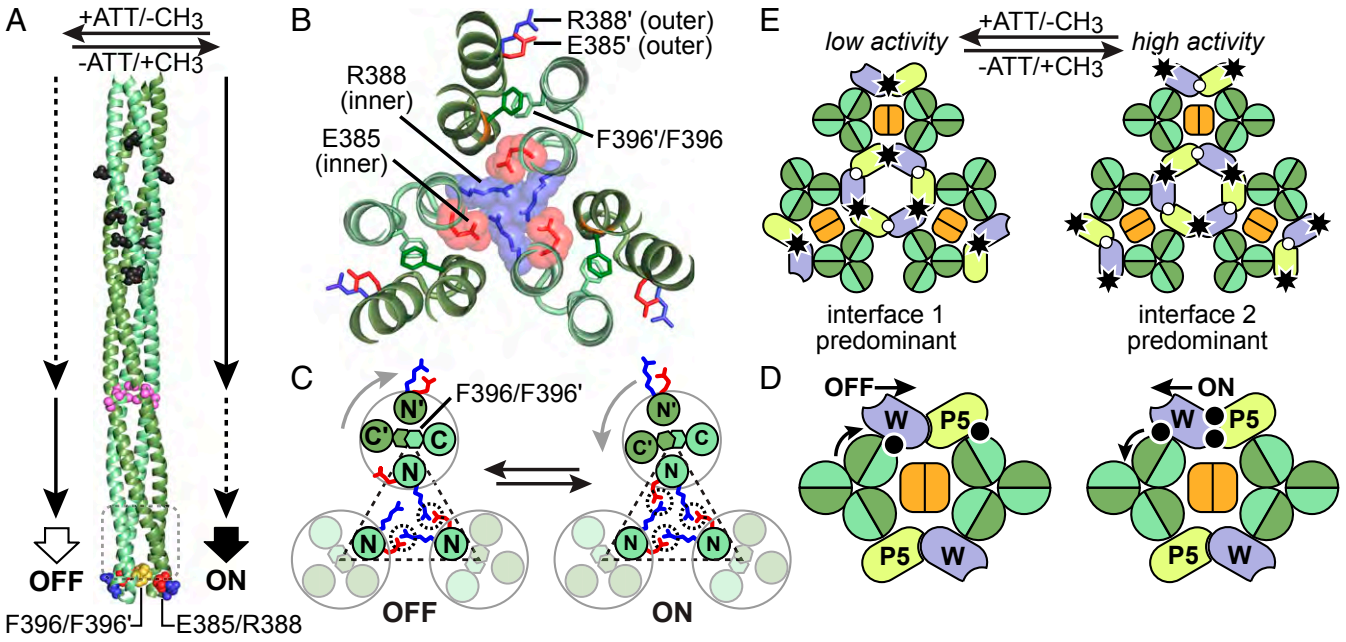

Fig. 7. Two-state model of Tsr hairpin tip signaling. (*A*) Stimulus and adaptational control of receptor tip signals. The backbone structure of a Tsr dimer from the HAMP-MH bundle junction (*Upper*) to the hairpin tip (*Lower*). Subunits are colored light and dark green. Side-chain atoms of key residues are as follows: adaptation sites (black); glycine hinge (cyan); F396 (yellow); E385 (red); R388 (blue). The dashed box outlines the tip region that promotes trimer and core complex assembly. Vertical arrows indicate structural inputs to the tip: weakened helix-packing (dashed lines); strengthened helix-packing (solid lines). (*B*) Cross-section of the Tsr trimer of dimers viewed from the membrane toward the tip; atomic coordinates from Protein Data Bank ID code 1QU7 (5). The N-helices of the light green subunits interact at the trimer axis. The F396 and F396′ residues stabilize the dimer tips through an aromatic stacking interaction between the C and C′ helices at the subunit interfaces. (*C*) Cartoon depictions of the trimer cross-section in *B* showing proposed conformations for alternative output states. The N-helices of the dark green subunits interact with the CheW protein and the CheA.P5 domain in core complexes. Helix motions that accompany F396/F396′ stacking changes are shown for the trimer member that binds CheW in the core complex. Dashed triangles enclose the N-helices at the trimer axis. E385 (red) and R388 (blue) side chains are shown as sticks with dashed circles indicating their ionic interactions at the trimer axis. (*D*) Signal-related conformational changes in the receptor core complex. The receptor directly bound to CheW most likely controls CheA activity by modulating CheW-CheA.P5 interface 1 (16, 47). Semicircles indicate the inner (light green) and outer (dark green) subunits of each receptor dimer. Black circles indicate cysteine reporter sites that show signal-dependent cross-linking efficiencies: receptor-CheW (70); CheW-CheA.P5 (47); CheA.P5-receptor (44). (*E*) Model of activity-dependent changes in array connectivity. The relative strengths of interface 1 and interface 2 interactions within and between core signaling units may shift with activity state, reflecting the interplay of attractant stimuli and adaptational modifications. Open circles denote weak interfaces; black stars denote strong interfaces. Colors for the CheW and CheA.P5 domains correspond to those in *D*. Semicircles indicate the inner (light green) and outer (dark green) subunits of each receptor dimer.

control (E385F|Y|W|H); inverted response to adaptational modification (E385I|L|M); labile kinase activities (R388V|M|F); and locked-ON (E385K|R|D|C) or locked-OFF (E385P; R388D|E) outputs. Some of these mutant receptors might have more dynamic hairpin tips, but we contend that their mutant behaviors arise mainly through substantial stabilization or destabilization of one native tip conformation and/or from being trapped in a nonnative tip structure, and not from a change in tip dynamic properties per se. The slow-response (E385N|G), partial control (E385F|Y|W|H), and inverted control (E385I|L|M) receptors seem to be defective to varying extents in reaching the native attractant-induced OFF conformation (see below), whereas the labile activities of the R388V|M|F receptors probably reflect serine-induced rearrangements that trap the mutant tips in the OFF conformation (see below).

Structural Bases for Mutant Signaling Properties. Structural features of the two-state tip model can explain E385* and R388* signaling defects. We assume that those signaling defects arise mainly from structural changes at the trimer axis location (Fig. 7*B*), but cannot rule out the possibility of additional signaling contributions from the E385 and R388 residues in their outer locations, for example, through a noncritical interaction with receptor-bound CheW.

In wild-type Tsr, the E385-R388 salt bridge would stabilize the ON-state F396 stacking arrangement, whereas dissipation of the salt-bridge connection would favor the alternative OFF-state stacking arrangement (Fig. 7*C*). Whether the members of a trimer are conformationally coupled and shift in synchrony as a single allosteric entity remains an open question. This may not be the case because attractant responses of individual core units have Hill coefficients below 2 (16, 34). In any event, coupled movements of the receptors are not essential to the model, so we consider only the structural changes in one member of a trimer (Fig. 7*C*). The signal-state conformational shifts are accompanied by rotation of three helices relative to the N-helix, whose position may be fixed through extensive contacts with the N-helices at the trimer axis (20). Viewed from the membrane toward the tip, the direction of rotation is counterclockwise in the ON state and clockwise in the OFF state (Fig. 7*C*). These rotational motions are most likely responsible for CheA activity control (see below). Because the E385-R388 salt bridge itself is not critical to the kinase-ON state, the key difference between the ON and OFF states could be the configuration of the E385 side chain at the trimer axis. In the wild-type ON state, the salt bridge positions the E385 side chain away from the adjacent C′-helix, whereas in the OFF state, a less-constrained E385 side chain could impinge on its C′-helix neighbor, promoting clockwise rotation of the other helices (Fig. 7*C*).

The side-chain methyl groups of the E385A|T|V receptors probably pack preferentially against the C′-helix to promote clockwise rotation and OFF-shifted output, but they might also engage the aliphatic portion of the R388 side chain to promote occasional counterclockwise rotation and kinase-ON ouput. The

polar side-chain character of the E385S|Q receptors could promote counterclockwise rotation and ON-shifted output through H-bonding interactions with the charged group of the R388 side chain. Those amino acid replacements might be small enough to allow occasional interactions with the C′-helix that trigger shifts to the OFF-state.

The small side chains of the R388A|V|T receptors produce OFF-shifted output, perhaps by occupying the apolar E385 cavity without steric hindrance. The mutant side chains of the R388G|W receptors, which produce ON-shifted output, would probably have less affinity for the E385 cavity. In contrast, the labile kinase activity of the R388V|M|F receptors could be caused by rearrangement of their hydrophobic side chains in the apolar environment around E385, augmented by serine-induced shifts to the OFF conformation. The acidic side chains of the locked-OFF R388D|E receptors, although solvent exposed, might engender charge-repulsion effects that constrain the acidic E385 side chain to the OFF-state conformation.

The slow-responding, ON-shifted E385G receptor, lacking a side-chain contribution, is most likely defective in stabilizing the OFF conformation. The E385N receptor has similar signaling properties, but was a very poor substrate for CheR, suggesting that its short, polar side chain might actively destabilize the OFF state and at the same time stabilize an ON conformation through H bonding with R388. The locked-ON output of E385D probably represents a more extreme example of such a dual effect. That receptor was refractory to CheR but in the QEQEE modification state produced only intermediate levels of kinase activity. In a host with both adaptation enzymes, its kinase activity increased considerably but remained unresponsive to serine. We suggest that the aspartic acid side chain destabilizes the OFF conformation and that it forms a salt-bridge connection with R388, but one that distorts the native ON conformation due to its shorter length. CheB-mediated deamidation probably shifts the receptor away from that suboptimal ON conformation toward the native ON state. The locked-ON E385K|R receptors also appear to have suboptimal ON conformations, perhaps due to charge repulsion by R388. Consistent with this idea, charge reversals at both the 385 and 388 positions produced more normal signaling properties.

The inverted adaptational responses of the E385I|L|M receptors represent further examples of suboptimal ON conformations. E385I had moderate kinase activity, but CheR/CheB substrate properties characteristic of an OFF-shifted receptor. E385L is a normal substrate for both enzymes, whereas E385M was a poor CheR substrate. The aliphatic side chains at these mutant sites may each pack a bit differently into the E385 cavity, constraining the receptor to one or several nonnative output conformations. The E385F|Y|W|H receptors produced near wild-type levels of kinase activity but responded very poorly to serine stimuli. Conceivably, a large planar side chain at residue 385 hinders the structural shifts needed to reach the OFF conformation. The locked-OFF E385P receptor was a poor substrate for both CheR and CheB and appears to be even more conformationally challenged. Its destabilized tip helices might adopt a relatively neutral conformation that neither activates the CheA kinase nor provides sufficient structural feedback to allow the methylation helices to achieve a preferred substrate state for either adaptation enzyme.

Array-Influenced Signaling Properties of E385* and R388* Receptors. The aberrant signaling properties of the E385F|Y and E385N|G receptors changed dramatically in a CheW-X3 host that could not make interface 2 array connections: The partial-control E385F|Y receptors were able to down-regulate all of their kinase activity; the slow-response E385N|G receptors acquired normal response kinetics. These behavior changes imply that interface 2 connections impair the signaling responses of partial-control and slow-response mutant receptors. We suggest that the large signaling teams formed in array-competent cells resist down-regulation by both classes of mutant receptors. The partial-control receptors may only control the kinase activity from a minority fraction of small signaling teams in the array. The mutant receptors cannot initiate signaling shifts in more highly coupled signaling teams. The slow-response receptors eventually control all signaling units in the array but may depend on relatively slow stimulus-induced changes in signal team size for effective kinase down-regulation.

Labile-activity (R388V|M|F) receptors and one partial-control receptor (E385W) produced no kinase activity in the CheW-X3 host. The interface 2 connections formed between core complexes during array assembly in the CheW+ host evidently contribute to their ON-state activity. Perhaps serine stimuli weaken or break those array connections in labile-activity receptors, trapping them in conformations that disfavor reestablishment of interface 2 array connections.

Activity-Dependent Changes in Array Connectivity. The array-influenced signaling behaviors of mutant receptors probably reflect activity-dependent changes in array connectivity that also occur in wild-type signaling complexes (31–33, 65–68). OFF-shifting stimuli and adaptational modifications seem to reduce signal team size; ON-shifting stimuli and receptor methylation increase signal team size (31, 32). These changes take place on a relatively slow timescale (33, 65, 66, 68), similar to the rate of kinase down-regulation by a slow-response receptor. We suggest that this array remodeling process involves a reciprocal tradeoff in the potencies of interface 1 and interface 2 array contacts (Fig. 7*E*). In signaling complexes with low kinase activity, interface 1 predominates, limiting the connectivity between signaling units. In high-activity arrays, interface 2 predominates, extending connections between signaling units and weakening the interface 1 connections within signaling units. This model implies that a strong interface 1 connection in a core complex inhibits its kinase activity, whereas a weaker or transient connection promotes kinase activity. Natale et al. (47) described attractant-induced reductions in S-S cross-linking between cysteine reporters at apposed CheW and CheA.P5 residues that they interpreted as evidence of a weakened interface 1 in the OFF state. However, it is equally possible that those interface 1 reporter sites become less mobile in the OFF state, thereby reducing productive collisions between them.

The two-state model of receptor tip output suggests a simple mechanism for activity-dependent modulation of interface 1 and 2 interactions (Fig. 7*D*). In core signaling units, one dimer in each trimer engages a CheW molecule (69), which, in turn, is bound through interface 1 to the P5 domain (47) in one subunit of the CheA dimer (Figs. 1 *B* and *C* and 7*D*). Viewed from the membrane toward the tip, in the ON state the CheW-bound N′-helix rotates counterclockwise (Fig. 7*C*), which could strain the interface 1 interaction between CheW and its P5 partner and enhance their interface 2 interactions (Fig. 7*D*). In the OFF state, the CheW-bound receptor helix rotates clockwise, thereby straining the interface 2 links and enhancing interface 1 interactions. These predicted signaling motions of CheW and the CheA.P5 domain relative to receptor molecules in a core complex are respectively consistent with in vivo (70) and in vitro (44) cross-linking results (Fig. 7*D*) and support the idea that interface 1 and interface 2 contacts change the conformation or dynamic motion of the CheA.P5 domain to govern CheA activity. That control mechanism remains to be elucidated.

Cooperativity and Adaptation Defects of Output-Shifted E385* and R388* Receptors. In an adaptation-deficient host, wild-type Tsr exhibits serine control responses with Hill coefficients of 10–20 (26, 71). In contrast, responses by the OFF-shifted E385A|V|T and R388A receptors were much less cooperative, consistent with signaling teams of smaller size predicted by the array-remodeling process. Conversely, the ON-shifted R388G|W receptors produced highly cooperative responses, consistent with large signaling teams. However, the ON-shifted E385S|Q receptors did not show high cooperativity responses. We speculate that these mutant receptors engender more team-to-team or

cell-to-cell variability in serine response thresholds, which would lead to ensemble FRET responses of apparent low cooperativity (65). Single-cell FRET kinase assays could resolve this issue (65, 66).

The output-shifted E385* receptors (A|V|T [OFF]; S|Q [ON]) exhibited better sensory adaptation ability than their R388* counterparts (E388A [OFF]; R388G|W [ON]). Mutant receptors of each output class exhibited comparable substrate properties for the CheR and CheB adaptation enzymes, so it is not clear why their behaviors differ in a host with both adaptation enzymes. Further experiments will be needed to clarify the mechanistic basis for these differences.

Key Findings and Outstanding Questions. The mutant receptor behaviors characterized in this study suggest that the helical hairpin tips of MCP-family chemoreceptors are two-state signaling devices. How tip conformation responds to structural inputs from the methylation helix bundle remains an open question. The intervening flexible bundle and glycine hinge play important roles in that signaling process (3, 59, 60, 72). The unusual array-dependent signaling behaviors of some E385* and R388* receptors suggest a general mechanism by which chemoeffector stimuli and adaptational modifications influence the cooperative connections between core signaling units. The array remodeling process may involve activity-dependent changes in the relative strengths of interface 1 and 2 interactions between the CheW and CheA.P5 components of receptor signaling complexes. This mechanistic model makes testable predictions to guide follow-up experiments on signaling in chemoreceptor arrays.

Materials and Methods

Bacterial Strains and Growth Conditions. All strains used in the study were derivatives of *E. coli* strain RP437 (73) and are listed in *SI Appendix*, Table S1. Bacterial cultures were grown in tryptone broth (10 g/L tryptone; 5 g/L NaCl) at 30 °C with shaking.

Plasmids. Plasmids used in this study were as follows: pKG116 (74), a derivative of pACYC184 (75) that confers chloramphenicol resistance and has a sodium salicylate-inducible cloning site; FRET reporter plasmid pRZ30, a derivative of pKG116 that expresses *cheY-yfp* and *cheZ-cfp* gene fusions under salicylate control (71); pPA114, a pKG116 derivative that expresses wild-type *tsr* (6); pVS88, a derivative of pTrc99A that expresses *cheY-yfp* and *cheZ-cfp* under IPTG-inducible control (24); and pRR53, a pRR48 derivative that expresses wild-type *tsr* under IPTG control (6).

Site-Directed Mutagenesis. Mutations in plasmids pRR53 and pPA114 were generated by QuikChange PCR mutagenesis and confirmed by sequencing the entire *tsr* coding region (21).

Expression Levels of Mutant Tsr Proteins. Tsr expression from pPA114 and pRR53 derivatives was analyzed in strain UU2610 ($CheR^-$ $CheB^-$). Protein samples were prepared and analyzed by sodium dodecyl sulfate-containing polyacrylamide gel electrophoresis (SDS/PAGE) and immunoblotting as previously described (76). Quantification of protein levels was performed with ImageJ as described (22).

Chemotaxis Assays. UU2612 strains carrying pPA114 Tsr-E385* derivatives were assessed for chemotactic ability on tryptone soft-agar plates containing 12.5 μg/mL chloramphenicol and 0.6 μM sodium salicylate as previously described (6). Plates were incubated at 30–32.5 °C for 6–8 h.

Clustering Assays. Mutant pRR53 and pPA114 derivatives were tested in strain UU3046, which expresses a CheA::mYFP fusion protein. Cells were grown to midexponential phase at 30 °C in tryptone broth containing 12.5 μg/mL chloramphenicol and 0.6 μM NaSal inducer for pPA114 derivatives, or 50 μg/mL ampicillin and 100 μM IPTG inducer for pRR53 derivatives. Cells were analyzed by fluorescence microscopy as previously described (6).

Receptor Modification Assays. Strains UU2610, UU2611, and UU2632 carrying mutant *tsr* plasmids were grown and induced for Tsr expression as described above for clustering assays. Cells were washed twice, and one sample was treated with 10 mM L-serine for 30 min at 30 °C. Cell lysates were analyzed by SDS/PAGE, and Tsr protomers in different modifications states were visualized by immunoblotting as previously described (77).

FRET Kinase Assays. The assay protocol and data analysis followed the procedures previously described in detail (25, 71). Briefly, FRET signals were collected from cells expressing the reporter pair CheY-YFP and CheZ-CFP from plasmid pRZ30 (for pRR53 derivatives) or from plasmid pVS88 (for pPA114 derivatives). FRET data were processed and fitted to a multisite Hill equation using KaleidaGraph 4.5 software to obtain $K_{1/2}$ and Hill coefficient values. Maximal kinase activities were calculated from the FRET changes to a saturating serine stimulus (25) or to treatment with 3 mM KCN (71), which collapses cellular ATP, the phosphodonor for the CheA autophosphorylation reaction.

Protein Structural Display. Structure images were prepared with PyMOL (Mac) software.

ACKNOWLEDGMENTS. We thank Run-Zhi Lai for helpful discussions and experimental suggestions during the early phases of this project, Keith Cassidy for an MD-generated model of the Tsr dimer, Davi Ortega for insightful mechanistic suggestions during the preparation of the manuscript, and Caralyn Flack and Claudia Studdert for editorial comments on the manuscript. Q.G. received fellowship support (2017YFD0500800) from the National Key Research and Development Program of China and fellowship support (CARS-42-17) from the China Agricultural Research System. This work was supported by Research Grant GM19559 (to J.S.P.) from the National Institute of General Medical Sciences. The Protein-DNA Core Facility at the University of Utah receives support from National Cancer Institute Grant CA42014 to the Huntsman Cancer Institute.

1. G. L. Hazelbauer, J. J. Falke, J. S. Parkinson, Bacterial chemoreceptors: High-performance signaling in networked arrays. *Trends Biochem. Sci.* **33**, 9–19 (2008).
2. J. S. Parkinson, G. L. Hazelbauer, J. J. Falke, Signaling and sensory adaptation in *Escherichia coli* chemoreceptors: 2015 update. *Trends Microbiol.* **23**, 257–266 (2015).
3. R. P. Alexander, I. B. Zhulin, Evolutionary genomics reveals conserved structural determinants of signaling and adaptation in microbial chemoreceptors. *Proc. Natl. Acad. Sci. U.S.A.* **104**, 2885–2890 (2007).
4. M. Hulko *et al*., The HAMP domain structure implies helix rotation in transmembrane signaling. *Cell* **126**, 929–940 (2006).
5. K. K. Kim, H. Yokota, S. H. Kim, Four-helical-bundle structure of the cytoplasmic domain of a serine chemotaxis receptor. *Nature* **400**, 787–792 (1999).
6. P. Ames, C. A. Studdert, R. H. Reiser, J. S. Parkinson, Collaborative signaling by mixed chemoreceptor teams in *Escherichia coli*. *Proc. Natl. Acad. Sci. U.S.A.* **99**, 7060–7065 (2002).
7. C. A. Studdert, J. S. Parkinson, Crosslinking snapshots of bacterial chemoreceptor squads. *Proc. Natl. Acad. Sci. U.S.A.* **101**, 2117–2122 (2004).
8. M. Li, G. L. Hazelbauer, Core unit of chemotaxis signaling complexes. *Proc. Natl. Acad. Sci. U.S.A.* **108**, 9390–9395 (2011).
9. J. Liu *et al*., Molecular architecture of chemoreceptor arrays revealed by cryoelectron tomography of *Escherichia coli* minicells. *Proc. Natl. Acad. Sci. U.S.A.* **109**, E1481–E1488 (2012).
10. A. Briegel *et al*., Bacterial chemoreceptor arrays are hexagonally packed trimers of receptor dimers networked by rings of kinase and coupling proteins. *Proc. Natl. Acad. Sci. U.S.A.* **109**, 3766–3771 (2012).
11. P. Cluzel, M. Surette, S. Leibler, An ultrasensitive bacterial motor revealed by monitoring signaling proteins in single cells. *Science* **287**, 1652–1655 (2000).
12. S. Asakura, H. Honda, Two-state model for bacterial chemoreceptor proteins. The role of multiple methylation. *J. Mol. Biol.* **176**, 349–367 (1984).
13. N. Barkai, S. Leibler, Robustness in simple biochemical networks. *Nature* **387**, 913–917 (1997).
14. A. Borczuk, A. Staub, J. Stock, Demethylation of bacterial chemoreceptors is inhibited by attractant stimuli in the complete absence of the regulatory domain of the demethylating enzyme. *Biochem. Biophys. Res. Commun.* **141**, 918–923 (1986).
15. D. N. Amin, G. L. Hazelbauer, Chemoreceptors in signalling complexes: Shifted conformation and asymmetric coupling. *Mol. Microbiol.* **78**, 1313–1323 (2010).
16. G. E. Pinas, V. Frank, A. Vaknin, J. S. Parkinson, The source of high signal cooperativity in bacterial chemosensory arrays. *Proc. Natl. Acad. Sci. U.S.A.* **113**, 3335–3340 (2016).
17. V. Frank, G. E. Pinas, H. Cohen, J. S. Parkinson, A. Vaknin, Networked chemoreceptors benefit bacterial chemotaxis performance. *MBio* **7**, e01824-16 (2016).
18. C. K. Cassidy *et al*., CryoEM and computer simulations reveal a novel kinase conformational switch in bacterial chemotaxis signaling. *eLife* **4**, e08419 (2015).
19. X. Li *et al*., The 3.2 A resolution structure of a receptor: CheA:CheW signaling complex defines overlapping binding sites and key residue interactions within bacterial chemosensory arrays. *Biochemistry* **52**, 3852–3865 (2013).
20. D. R. Ortega *et al*., A phenylalanine rotameric switch for signal-state control in bacterial chemoreceptors. *Nat. Commun.* **4**, 2881 (2013).
21. P. Ames, J. S. Parkinson, All-codon mutagenesis for structure-function sudies of chemotaxis signaling proteins. *Methods Mol. Biol.* **1729**, 79–85 (2018).
22. P. Mowery, J. B. Ostler, J. S. Parkinson, Different signaling roles of two conserved residues in the cytoplasmic hairpin tip of Tsr, the *Escherichia coli* serine chemoreceptor. *J. Bacteriol.* **190**, 8065–8074 (2008).

23. C. A. Studdert, J. S. Parkinson, Insights into the organization and dynamics of bacterial chemoreceptor clusters through *in vivo* crosslinking studies. *Proc. Natl. Acad. Sci. U.S.A.* **102**, 15623–15628 (2005).
24. V. Sourjik, H. C. Berg, Receptor sensitivity in bacterial chemotaxis. *Proc. Natl. Acad. Sci. U.S.A.* **99**, 123–127 (2002).
25. V. Sourjik, A. Vaknin, T. S. Shimizu, H. C. Berg, In vivo measurement by FRET of pathway activity in bacterial chemotaxis. *Methods Enzymol.* **423**, 365–391 (2007).
26. X. S. Han, J. S. Parkinson, An unorthodox sensory adaptation site in the *Escherichia coli* serine chemoreceptor. *J. Bacteriol.* **196**, 641–649 (2014).
27. T. S. Shimizu, Y. Tu, H. C. Berg, A modular gradient-sensing network for chemotaxis in *Escherichia coli* revealed by responses to time-varying stimuli. *Mol. Syst. Biol.* **6**, 382 (2010).
28. A. Boyd, M. I. Simon, Multiple electrophoretic forms of methyl-accepting chemotaxis proteins generated by stimulus-elicited methylation in *Escherichia coli*. *J. Bacteriol.* **143**, 809–815 (1980).
29. P. Engstrom, G. L. Hazelbauer, Multiple methylation of methyl-accepting chemotaxis proteins during adaptation of *E. coli* to chemical stimuli. *Cell* **20**, 165–171 (1980).
30. D. Chelsky, F. W. Dahlquist, Multiple sites of methylation in the methyl accepting chemotaxis proteins of *Escherichia coli*. *Prog. Clin. Biol. Res.* **63**, 371–381 (1981).
31. R. G. Endres *et al*., Variable sizes of *Escherichia coli* chemoreceptor signaling teams. *Mol. Syst. Biol.* **4**, 211 (2008).
32. C. H. Hansen, V. Sourjik, N. S. Wingreen, A dynamic-signaling-team model for chemotaxis receptors in *Escherichia coli*. *Proc. Natl. Acad. Sci. U.S.A.* **107**, 17170–17175 (2010).
33. V. Frank, A. Vaknin, Prolonged stimuli alter the bacterial chemosensory clusters. *Mol. Microbiol.* **88**, 634–644 (2013).
34. M. Li, G. L. Hazelbauer, Selective allosteric coupling in core chemotaxis signaling complexes. *Proc. Natl. Acad. Sci. U.S.A.* **111**, 15940–15945 (2014).
35. E. G. Ninfa, A. Stock, S. Mowbray, J. Stock, Reconstitution of the bacterial chemotaxis signal transduction system from purified components. *J. Biol. Chem.* **266**, 9764–9770 (1991).
36. K. A. Borkovich, N. Kaplan, J. F. Hess, M. I. Simon, Transmembrane signal transduction in bacterial chemotaxis involves ligand-dependent activation of phosphate group transfer. *Proc. Natl. Acad. Sci. U.S.A.* **86**, 1208–1212 (1989).
37. A. M. Bilwes, L. A. Alex, B. R. Crane, M. I. Simon, Structure of CheA, a signal-transducing histidine kinase. *Cell* **96**, 131–141 (1999).
38. A. R. Greenswag, A. Muok, X. Li, B. R. Crane, Conformational transitions that enable histidine kinase autophosphorylation and receptor array integration. *J. Mol. Biol.* **427**, 3890–3907 (2015).
39. X. Wang, C. Wu, A. Vu, J. E. Shea, F. W. Dahlquist, Computational and experimental analyses reveal the essential roles of interdomain linkers in the biological function of chemotaxis histidine kinase CheA. *J. Am. Chem. Soc.* **134**, 16107–16110 (2012).
40. S. L. Gloor, J. J. Falke, Thermal domain motions of CheA kinase in solution: Disulfide trapping reveals the motional constraints leading to trans-autophosphorylation. *Biochemistry* **48**, 3631–3644 (2009).
41. X. Wang *et al*., The linker between the dimerization and catalytic domains of the CheA histidine kinase propagates changes in structure and dynamics that are important for enzymatic activity. *Biochemistry* **53**, 855–861 (2014).
42. X. Ding, Q. He, F. Shen, F. W. Dahlquist, X. Wang, Regulatory role of an interdomain linker in the bacterial chemotaxis histidine kinase CheA. *J. Bacteriol.* **200**, e00052-18 (2018).
43. A. Briegel *et al*., The mobility of two kinase domains in the *Escherichia coli* chemoreceptor array varies with signalling state. *Mol. Microbiol.* **89**, 831–841 (2013).
44. K. N. Piasta, C. J. Ulliman, P. F. Slivka, B. R. Crane, J. J. Falke, Defining a key receptor-CheA kinase contact and elucidating its function in the membrane-bound bacterial chemosensory array: A disulfide mapping and TAM-IDS study. *Biochemistry* **52**, 3866–3880 (2013).
45. X. Wang, A. Vu, K. Lee, F. W. Dahlquist, CheA-receptor interaction sites in bacterial chemotaxis. *J. Mol. Biol.* **422**, 282–290 (2012).
46. G. E. Piñas, M. D. DeSantis, J. S. Parkinson, Noncritical sgnaling role of a knase-receptor iteraction surface in the *Escherichia coli* chemosensory core complex. *J. Mol. Biol.* **430**, 1051–1064 (2018).
47. A. M. Natale, J. L. Duplantis, K. N. Piasta, J. J. Falke, Structure, function, and on-off switching of a core unit contact between CheA kinase and CheW adaptor protein in the bacterial chemosensory array: A disulfide mapping and mutagenesis study. *Biochemistry* **52**, 7753–7765 (2013).
48. J. S. Parkinson, Signaling mechanisms of HAMP domains in chemoreceptors and sensor kinases. *Annu. Rev. Microbiol.* **64**, 101–122 (2010).
49. Q. Zhou, P. Ames, J. S. Parkinson, Mutational analyses of HAMP helices suggest a dynamic bundle model of input-output signalling in chemoreceptors. *Mol. Microbiol.* **73**, 801–814 (2009).
50. Q. Zhou, P. Ames, J. S. Parkinson, Biphasic control logic of HAMP domain signalling in the *Escherichia coli* serine chemoreceptor. *Mol. Microbiol.* **80**, 596–611 (2011).
51. N. Sukomon, J. Widom, P. P. Borbat, J. H. Freed, B. R. Crane, Stability and conformation of a chemoreceptor HAMP domain chimera correlates with signaling properties. *Biophys. J.* **112**, 1383–1395 (2017).
52. N. L. Bartelli, G. L. Hazelbauer, Differential backbone dynamics of companion helices in the extended helical coiled-coil domain of a bacterial chemoreceptor. *Protein Sci.* **24**, 1764–1776 (2015).
53. N. L. Bartelli, G. L. Hazelbauer, Bacterial chemoreceptor dynamics: Helical stability in the cytoplasmic domain varies with functional segment and adaptational modification. *J. Mol. Biol.* **428**, 3789–3804 (2016).
54. D. J. Starrett, J. J. Falke, Adaptation mechanism of the aspartate receptor: Electrostatics of the adaptation subdomain play a key role in modulating kinase activity. *Biochemistry* **44**, 1550–1560 (2005).
55. M. Kashefi, L. K. Thompson, Signaling-related mobility changes in bacterial chemotaxis receptors revealed by solid-state NMR. *J. Phys. Chem. B* **121**, 8693–8705 (2017).
56. H. U. Ferris, K. Zeth, M. Hulko, S. Dunin-Horkawicz, A. N. Lupas, Axial helix rotation as a mechanism for signal regulation inferred from the crystallographic analysis of the *E. coli* serine chemoreceptor. *J. Struct. Biol.* **186**, 349–356 (2014).
57. S. E. Winston, R. Mehan, J. J. Falke, Evidence that the adaptation region of the aspartate receptor is a dynamic four-helix bundle: Cysteine and disulfide scanning studies. *Biochemistry* **44**, 12655–12666 (2005).
58. K. E. Swain, M. A. Gonzalez, J. J. Falke, Engineered socket study of signaling through a four-helix bundle: Evidence for a yin-yang mechanism in the kinase control module of the aspartate receptor. *Biochemistry* **48**, 9266–9277 (2009).
59. M. D. Coleman, R. B. Bass, R. S. Mehan, J. J. Falke, Conserved glycine residues in the cytoplasmic domain of the aspartate receptor play essential roles in kinase coupling and on-off switching. *Biochemistry* **44**, 7687–7695 (2005).
60. A. Pedetta, D. A. Massazza, M. K. Herrera Seitz, C. A. Studdert, Mutational replacements at the "glycine hinge" of the *Escherichia coli* chemoreceptor Tsr support a signaling role for the C-Helix residue. *Biochemistry* **56**, 3850–3862 (2017).
61. N. L. Bartelli, G. L. Hazelbauer, Direct evidence that the carboxyl-terminal sequence of a bacterial chemoreceptor is an unstructured linker and enzyme tether. *Protein Sci.* **20**, 1856–1866 (2011).
62. D. Samanta, P. P. Borbat, B. Dzikovski, J. H. Freed, B. R. Crane, Bacterial chemoreceptor dynamics correlate with activity state and are coupled over long distances. *Proc. Natl. Acad. Sci. U.S.A.* **112**, 2455–2460 (2015).
63. S. S. Koshy, X. Li, S. J. Eyles, R. M. Weis, L. K. Thompson, Hydrogen exchange differences between chemoreceptor signaling complexes localize to functionally important subdomains. *Biochemistry* **53**, 7755–7764 (2014).
64. K. K. Gosink, Y. Zhao, J. S. Parkinson, Mutational analysis of N381, a key trimer contact residue in Tsr, the *Escherichia coli* serine chemoreceptor. *J. Bacteriol.* **193**, 6452–6460 (2011).
65. J. M. Keegstra *et al*., Phenotypic diversity and temporal variability in a bacterial signaling network revealed by single-cell FRET. *eLife* **6**, e27455 (2017).
66. R. Colin, C. Rosazza, A. Vaknin, V. Sourjik, Multiple sources of slow activity fluctuations in a bacterial chemosensory network. *eLife* **6**, e26796 (2017).
67. Y. Tu, Quantitative modeling of bacterial chemotaxis: Signal amplification and accurate adaptation. *Annu. Rev. Biophys.* **42**, 337–359 (2013).
68. A. Vaknin, H. C. Berg, Physical responses of bacterial chemoreceptors. *J. Mol. Biol.* **366**, 1416–1423 (2007).
69. A. Vu, X. Wang, H. Zhou, F. W. Dahlquist, The receptor-CheW binding interface in bacterial chemotaxis. *J. Mol. Biol.* **415**, 759–767 (2012).
70. A. Pedetta, J. S. Parkinson, C. A. Studdert, Signalling-dependent interactions between the kinase-coupling protein CheW and chemoreceptors in living cells. *Mol. Microbiol.* **93**, 1144–1155 (2014).
71. R. Z. Lai, J. S. Parkinson, Functional suppression of HAMP domain signaling defects in the *E. coli* serine chemoreceptor. *J. Mol. Biol.* **426**, 3642–3655 (2014).
72. N. Akkaladevi, F. Bunyak, D. Stalla, T. A. White, G. L. Hazelbauer, Flexible hinges in bacterial chemoreceptors. *J. Bacteriol.* **200**, e00593-17 (2018).
73. J. S. Parkinson, S. E. Houts, Isolation and behavior of *Escherichia coli* deletion mutants lacking chemotaxis functions. *J. Bacteriol.* **151**, 106–113 (1982).
74. K. K. Gosink, M. Buron-Barral, J. S. Parkinson, Signaling interactions between the aerotaxis transducer Aer and heterologous chemoreceptors in *Escherichia coli*. *J. Bacteriol.* **188**, 3487–3493 (2006).
75. A. C. Y. Chang, S. N. Cohen, Construction and characterization of amplifiable multicopy DNA cloning vehicles derived from the p15A cryptic miniplasmid. *J. Bacteriol.* **134**, 1141–1156 (1978).
76. P. Ames, J. S. Parkinson, Constitutively signaling fragments of Tsr, the *Escherichia coli* serine chemoreceptor. *J. Bacteriol.* **176**, 6340–6348 (1994).
77. M. K. Slocum, J. S. Parkinson, Genetics of methyl-accepting chemotaxis proteins in *Escherichia coli*: Null phenotypes of the *tar* and *tap* genes. *J. Bacteriol.* **163**, 586–594 (1985).
78. R. Z. Lai, K. K. Gosink, J. S. Parkinson, Signaling consequences of structural lesions that alter the stability of chemoreceptor timers of dimers. *J. Mol. Biol.* **429**, 823–835 (2017).
79. C. E. Flack, J. S. Parkinson, A zipped-helix cap potentiates HAMP domain control of chemoreceptor signaling. *Proc. Natl. Acad. Sci. U.S.A.* **115**, E3519–E3528 (2018).
80. P. Ames, S. Hunter, J. S. Parkinson, Evidence for a helix-clutch mechanism of transmembrane signaling in a bacterial chemoreceptor. *J. Mol. Biol.* **428**, 3776–3788 (2016).
81. S. Kitanovic, P. Ames, J. S. Parkinson, A trigger residue for transmembrane signaling in the Escherichia coli serine chemoreceptor. *J. Bacteriol.* **197**, 2568–2579 (2015).

PNAS
www.pnas.org

Supplementary Information for

Conformational shifts in a chemoreceptor helical hairpin control kinase signaling in *Escherichia coli*

Qun Gao[a,b], Anchun Cheng[a], and John S. Parkinson[b,*]

[a] College of Veterinary Medicine, Sichuan Agricultural University, Chengdu, China
[b] School of Biological Sciences, University of Utah, Salt Lake City, Utah 84112 USA

John S. Parkinson
Email: parkinson@biology.utah.edu

This PDF file includes:

Figs. S1 to S5
Tables S1 to S4
References for SI reference citations

www.pnas.org/cgi/doi/10.1073/pnas.1902521116

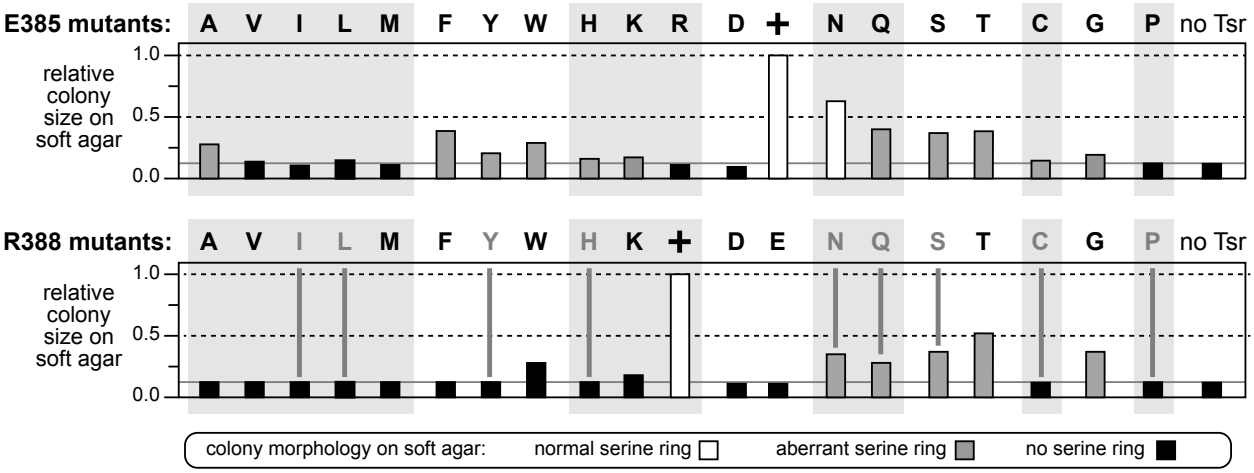

Fig. S1 Chemotaxis performance of Tsr-R388* and Tsr-E385* receptors. Amino acid replacements in the mutant receptors, grouped by sidechain chemical character, are indicated with one-letter designations; + = wild-type residue. Chemotaxis performance of pPA114-E385*, pRR53-R388*, or pCS53-R388* (gray vertical lines) derivatives was measured in UU2612 on tryptone soft agar, as detailed in Materials & Methods. In our lab the standard deviation of these measurements is less than ±10%. Dashed lines at 0.5 and 1.0 are simply to assist comparisons. The gray line at 0.15 indicates the colony size of UU2612 containing a control plasmid (pKG116 or pRR48).

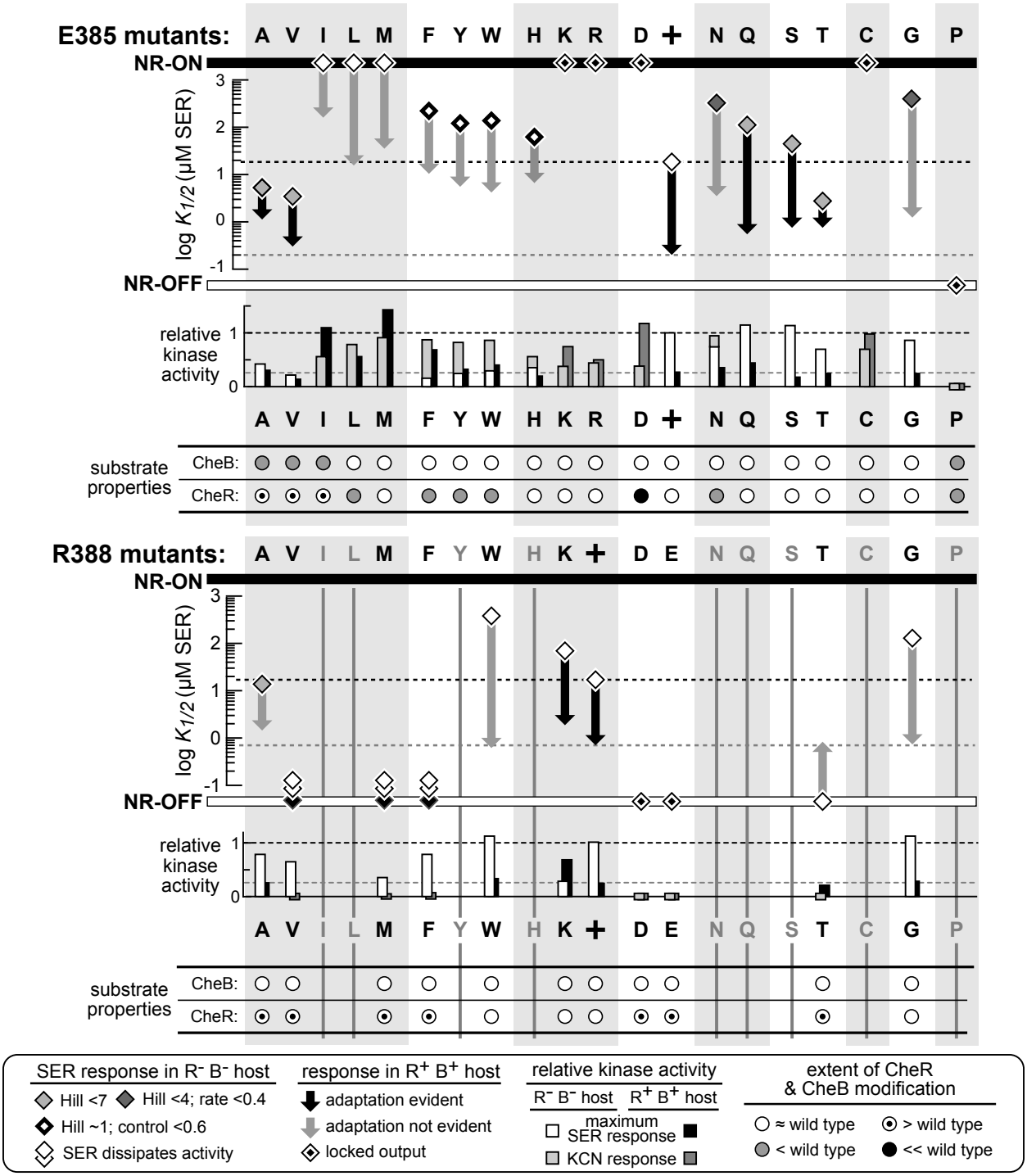

Fig. S2 Signaling properties of Tsr-E385* and Tsr-R388* receptors. Amino acid replacements in mutant receptors, grouped by sidechain chemical character, are indicated with one-letter designations; + = wild-type residue. Top and middle panels in each figure show data from FRET kinase assays. In our lab, standard deviations for $K_{1/2}$ measurements are typically less than ±25%; those for Hill coefficients and kinase activities are typically less than ±50% (1-8). Dashed horizontal lines indicate values for wild-type Tsr in the UU2567 (R-B-; black lines) and UU2700 (R+B+; gray lines) hosts. All kinase activities are normalized to that of wild-type Tsr in UU2567 and represent the

larger of the activity inhibited by a saturating serine stimulus (white and black bars) or by KCN treatment (light gray and dark gray bars). Bottom panels in each figure summarize the extent of adaptational modifications, measured as described in Materials and Methods. Hill coefficients in UU2567 (see Tables S2 & S3) were classified as wild-type (open diamond); below 7 (gray diamond); below 4 and with a response time more than twice the wild-type (dark gray diamond) about 1 and with inhibition of less than 60% of kinase activity (diamond with thick black border).

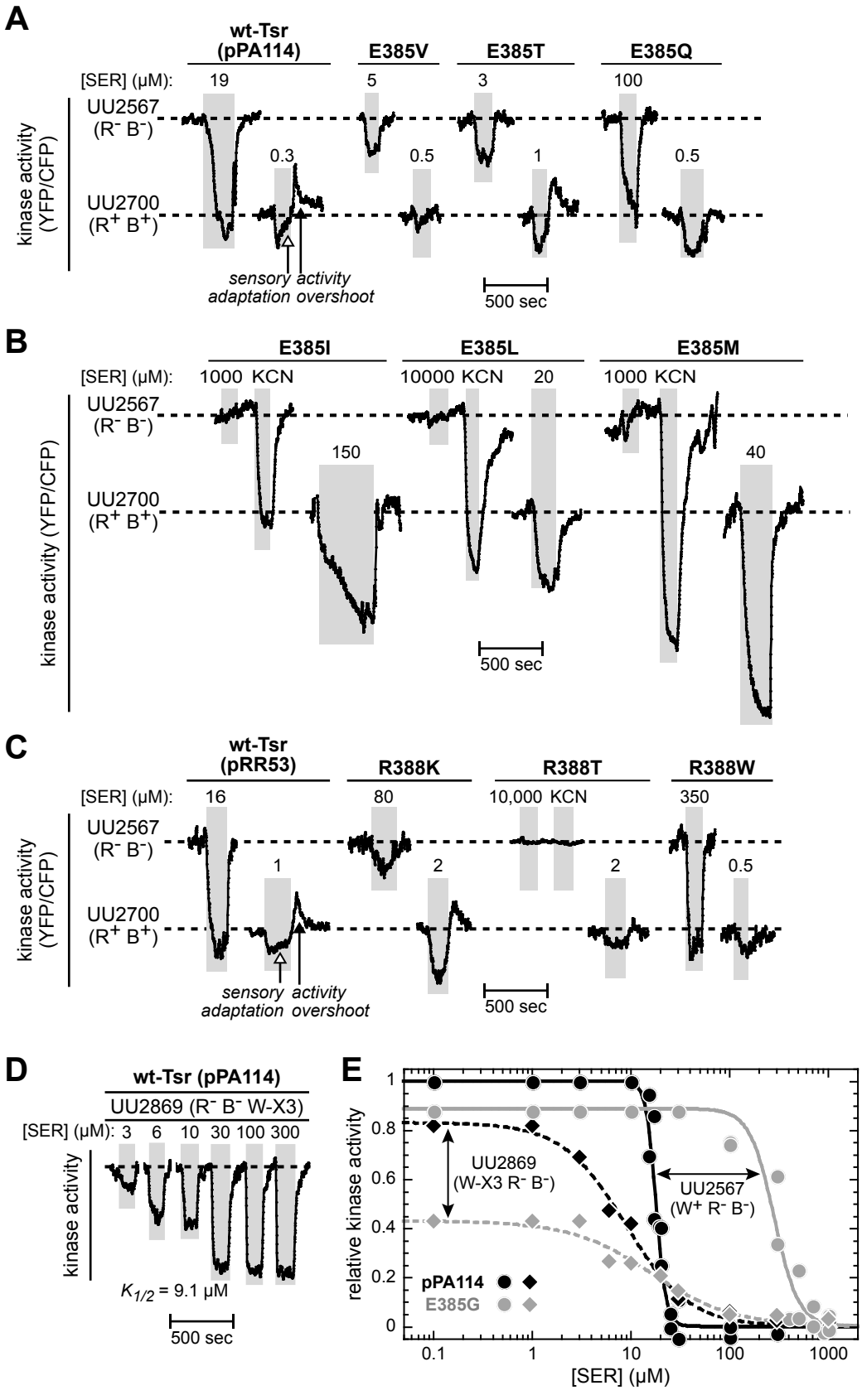

Fig. S3 Examples of E385*and R388* signaling behaviors in FRET kinase assays. Kinase responses are shown as changes in the pre-stimulus ratio of CheY-YFP to CheZ-CFP emission counts in FRET kinase assays. Dashed lines indicate relative baseline

activities in UU2567 (R-B-) and UU2700 (R+B+). All traces have the same activity and time scales. Gray rectangles indicate periods during which cells experienced the indicated concentrations of serine. Serine stimuli were near the $K_{1/2}$ concentrations in both hosts except as indicated below.

A. Output-shifted E385* receptors; see Fig. 2 and Fig. 3 for additional examples.

B. E385* receptors with paradoxical signaling properties; also see Fig. 2

C. Output-shifted R388* receptors; see Fig. 2 and Fig. 3 for additional examples.

D. Wild-type Tsr responses in UU2869 (adaptation-defective, array-defective).

E. Hill fits of dose-response data for wild-type Tsr and Tsr-E385G in array-competent (UU2567) and array-defective (UU2869) hosts lacking sensory adaptation enzymes.

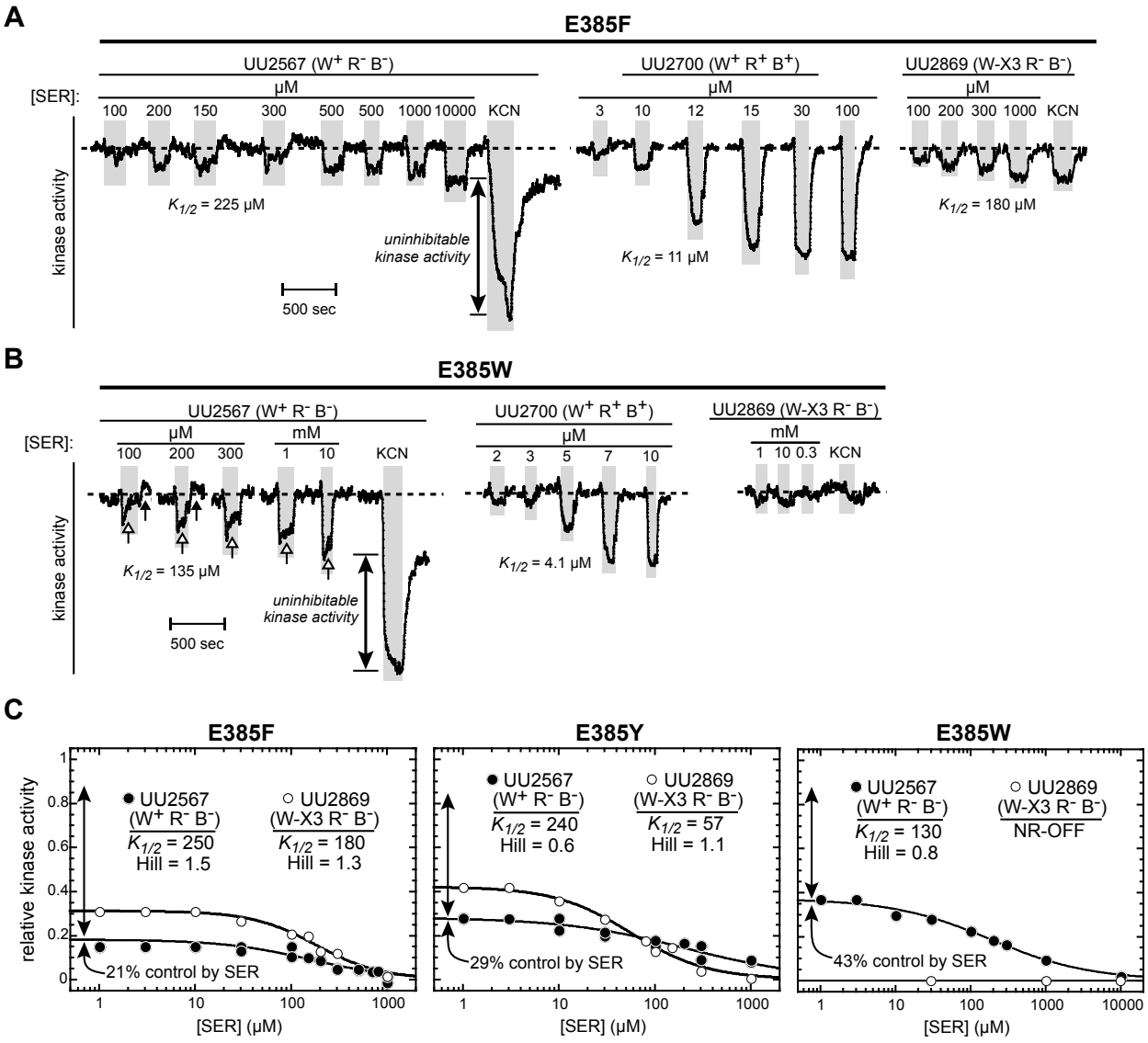

Fig. S4 Signaling properties of E385* receptors exhibiting partial kinase control.

A. Kinase control responses of Tsr-E385F in array-competent (UU2567; UU2700) and array-defective (UU2869) hosts. Kinase activity responses are shown as changes in the pre-stimulus ratio of CheY-YFP to CheZ-CFP emission counts in FRET kinase assays. Gray rectangles indicate periods during which cells experienced the indicated concentrations of serine. Response traces were from the same experiment; gaps indicate serine concentration(s) omitted from the trace. The derived $K_{1/2}$ concentration is shown below the trace; other parameter values are given in panel D.

B. Kinase control responses of Tsr-E385W. Open and closed vertical arrows indicate adaptation-like behaviors in the host lacking adaptation enzymes. See panel A for other details.

C. Kinase control responses of Tsr-E385H in the UU2567 host. See panels A and B for details.

D. Hill fits of E385* serine responses. Each panel shows two Hill fits for serine responses from FRET kinase assays in receptor-less, adaptation-deficient hosts: UU2567 is array-

competent; UU2869 expresses a mutant form of CheW (CheW-X3) that abrogates interface 2 connections between core signaling units. The data for UU2567 responses (filled circles) come from two independent experiments with a single fit applied to all data points. The response parameters are the averaged values from two separate experimental fits (see Table S3). The data for UU2869 responses (unfilled circles) are in each case fits from a single experiment.

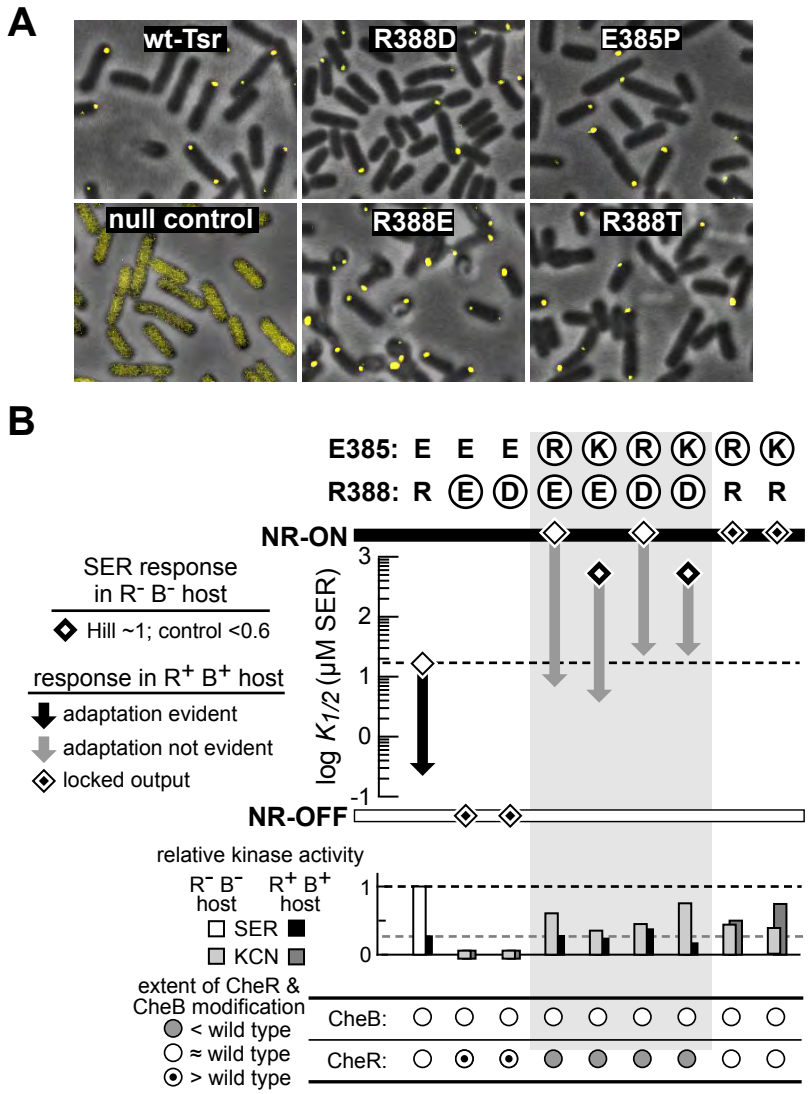

Fig. S5 Phenotypes of locked-output E385* and R388* receptors.

A. Core complex formation by kinase-OFF receptors. UU3046 (receptor-less, Δ*cheRBYZ cheA::myfp*) cells containing receptor plasmids were imaged by phase contrast and fluorescence microscopy as detailed in Materials and Methods. Panels show overlays of fluorescence and phase images. All fluorescence images were taken at the same exposure setting.

B. Signaling properties of single and double charge-reversal. Amino acids at residues 385 and 388 are indicated in single-letter designations with mutant replacements circled. Data from FRET kinase assays are summarized as in Fig. S2.

Table S1. Bacterial strains

Strain	relevant genotype	Ref
UU1250	*(tsr)Δ7028 (tar-tap)Δ5201 (trg)Δ100 aerΔ1*	(9)
UU1613	*tar-S364C (tsr)Δ7028 (trg)Δ100 (tap-cheB)Δ2234 (cheA-cheW)Δ2167*	(10)
UU1623	*(tsr)Δ7028 (tap)Δ3654 (trg)Δ100*	(11)
UU2610	*(tsr)Δ5547 (tar-cheB)Δ4346 (trg)Δ4543 aerΔ1*	(12)
UU2611	*(tsr)Δ5547 (tar-cheR)Δ4283 (trg)Δ4543 aerΔ1*	(12)
UU2612	*(tsr)Δ5547 (tar-tap)Δ4530 (trg)Δ4543 aerΔ1*	(12)
UU2632	*(tsr)Δ5547 (tar-tap)Δ4530 cheBΔ4345 (trg)Δ4543 aerΔ1*	(12)
UU2378	*tsr-T156K (tar-tap)Δ5201 (trg)Δ4543 aerΔ-1 ΔrecA*	(11)
UU2567	*(tsr)Δ5547 (trg)Δ4543 aerΔ1 (tar-cheZ)Δ4211 (cheY-cheZ)Δ1215*	(2)
UU2700	*(tsr)Δ5547 (tar-tap)Δ4530 (trg)Δ4543 aerΔ (cheY-cheZ)Δ1215*	(2)
UU2869	*(tsr)Δ5547 (trg)Δ4543 aerΔ1 (tar-cheZ)Δ4211 (cheY-cheZ)Δ1215 cheW-X3(R117D/E121R/F122S)*	(13)
UU3046	*(tsr)Δ5547 (trg)Δ4543 aerΔ1 (tar-cheZ)Δ4211 cheA::mYFP*	this work

Table S2. Properties of Tsr-E385* mutants

	fraction of wild-type		serine responses in UU2567 (CheR$^-$ CheB$^-$) [c]			serine responses in UU2700 (CheR$^+$ CheB$^+$) [c]		
E385*	taxis [a]	[CheA*] [b]	$K_{1/2}$	Hill	Act	$K_{1/2}$	Hill	Act
A	0.28 ± 0.01	1.25 ± 0.07	4.7	5.5	0.43	1.2	0.7	0.31
V	0.15 ± 0.01	0.70	3.6	4.9	0.22	0.3	1.9	0.14
I	0.10 ± 0.01	0.65	NR	NR	*0.57*	160	2.5	1.12
L	0.15 ± 0.06 [4]	0.95	NR	NR	*0.80*	17	2.6	0.57
M	0.11 ± 0.01	1.1	NR	NR	*0.93*	37	6.4	1.46
F	0.39 ± 0.02	0.80	250 ± 36	1.5 ± 0.5	0.16 / *0.89* [d]	11	9.5	0.70
Y	0.21 ± 0.01	0.85	240 ± 141	0.65 ± 0.2	0.25 / *0.84* [d]	5.4	2.0	0.33
W	0.29 ± 0.03	1.1	130 ± 5	0.8 ± 0.2	0.30 / *0.88* [d]	4.1	3.9	0.41
H	0.16 ± 0.01	0.85	160	0.9	0.36 / *0.57* [d]	7.0	2.0	0.20
K	0.17 ± 0.01	0.70	NR	NR	*0.40*	15	1.1	*0.76*
R	0.11 ± 0.01	0.90	NR	NR	*0.45*	NR	NR	*0.51*
D	0.09 ± 0.01	0.75	NR	NR	*0.39*	NR	NR	*1.57*
E (wt)	**1.0**	**1.0**	**18 ± 1.4**	**10 ± 3.4**	**1.00**	**0.2**	**1.6**	**0.27**
N	0.64 ± 0.03 [4]	0.55	260 ± 93 [3]	2.1 ± 1.4 [3]	0.76 / *0.97* [d]	3.7	2.9	0.36
Q	0.40 ± 0.06 [4]	0.60	110	6.6	1.17	0.6	1.1	0.45
S	0.37 ± 0.01	1.3	46	5.4	1.16	0.8	1.0	0.18
T	0.39 ± 0.03 [4]	1.0	2.8	3.5	0.71	0.6	1.8	0.25
C	0.15 ± 0.01	1.3	NR	NR	0.71	NR	NR	*1.00*
G	0.20 ± 0.01	1.0	300 ± 110	3.4 ± 0.6	0.88	1.2	6.8	0.25
P	0.10 ± 0.01	0.65	NR	NR	*0.0*	NR	NR	*0.0*

[a] Colony size produced by pPA114 Tsr-E385* plasmids in receptor-less host UU2612 (CheR$^+$ CheB$^+$) on tryptone soft agar plates incubated for 6-8 hours at 32.5°C. Values are averages and standard deviations of two or more [N] measurements relative to a wild-type control on the same plate.

[b] Intracellular level of mutant Tsr protein expressed by E385* plasmids in receptor-less host UU2610 (CheR$^-$ CheB$^-$), normalized to the wild-type level. Values for Tsr-E385A show the average and standard deviation from two independent expriments to illustrate the reproducibility of the measurements. For all other mutant proteins, values below 1.0 were rounded to the nearest 0.05 and values above 1.0 were rounded to the nearest 0.1.

[c] Data are from FRET-based dose-response experiments (see Methods for details). $K_{1/2}$ values are in μM serine units. Unless averaged from multiple experiments, $K_{1/2}$ and Hill values below 10 were rounded to the nearest 0.1, values above 10 were rounded to the nearest whole number, and values above 100 were rounded to the nearest 10. Kinase activities are the larger of the value obtained from the FRET change to a saturating serine stimulus or to 3 mM KCN treatment (italics). Kinase values are normalized to the wild type kinase activity in strain UU2567 (CheR$^-$ CheB$^-$). $K_{1/2}$ and Hill measurements with error values represent means and standard deviations based on two or more [N] independent experiments.

[d] First value is the activity inhibited by a saturating serine stimulus; italiciized value is the activity revealed by KCN treatment.

NR: no response to 10 mM serine

Table S3. Properties of Tsr-R388* mutants

	serine responses in UU2567 (CheR$^-$ CheB$^-$) [a]			serine responses in UU2700 (CheR$^+$ CheB$^+$) [a]		
R388*	$K_{1/2}$	Hill	Act	$K_{1/2}$	Hill	Act
A	13	2.2	0.79	1.4 ± 0.4 [3]	1.1 ± 0.4 [3]	0.35 ± 0.1 [3]
V	AD	AD	0.66	NR	NR	*0.0*
M	AD	AD	0.36	NR	NR	*0.0*
F	AD	AD	0.83 ± 0.12	NR	NR	*0.0*
W	340	17	1.11	0.6	3.1	0.34
K	70	10	0.28	1.7	2.1	0.72
R (wt)	**16**	**37**	**1.0**	**0.7**	**1.7**	**1.0**
D	NR	NR	*0.0*	NR	NR	*0.0*
E	NR	NR	*0.0*	NR	NR	*0.0*
T	NR	NR	*0.0*	2.1	0.9	0.21
G	120	8.8	1.11	0.65 ± 0.4 [3]	1.4 ± 0.3 [3]	0.35 ± 0.07 [3]

[a] Data are from FRET-based dose-response experiments (see Methods for details). $K_{1/2}$ values are in μM serine units. Unless averaged from multiple experiments, $K_{1/2}$ and Hill values below 10 were rounded to the nearest 0.1, values above 10 were rounded to the nearest whole number, and values above 100 were rounded to the nearest 10. Kinase activities are the larger of the value obtained from the FRET change to a saturating serine stimulus or to 3 mM KCN treatment (italics). Kinase values are normalized to the wild type kinase activity in strain UU2567 (CheR$^-$ CheB$^-$). Measurements with error values represent means and standard deviations based on two or more [N] independent experiments.

AD: Activity declined but did not recover after an initial serine stimulus.

NR: no response to 10 mM serine

Table S4. Signaling parameters of Tsr E385* and R388* receptors in a CheW-X3 host.

	serine responses in UU2869 (CheR$^-$ CheB$^-$ CheW-X3)		
Tsr mutant	$K_{1/2}$	Hill	Act
pPA114 (wt)	9.1	1.4	0.83
E385G	17	1.1	0.43
E385N	67	1.4	0.44
E385F	180	1.3	0.31
E385Y	57	1.1	0.42
E385W	NR	NR	*0.00*
R388V	NR	NR	*0.00*
R388M	NR	NR	*0.00*
R388F	NR	NR	*0.00*

Data are from FRET-based dose-response experiments (see Methods for details). $K_{1/2}$ values are in μM serine units. $K_{1/2}$ and Hill values below 10 were rounded to the nearest 0.1, values above 10 were rounded to the nearest whole number, and values above 100 were rounded to the nearest 10. Kinase activities are the larger of the value obtained from the FRET change to a saturating serine stimulus or to 3 mM KCN treatment (italics). Kinase values are normalized to the wild type kinase activity in strain UU2567 (CheR$^-$ CheB$^-$ CheW$^+$).

NR: no response to 10 mM serine

REFERENCES

1. Han XS & Parkinson JS (2014) An unorthodox sensory adaptation site in the *Escherichia coli* serine chemoreceptor. *J Bacteriol* 196:641-649.
2. Lai RZ & Parkinson JS (2014) Functional suppression of HAMP domain signaling defects in the *E. coli* serine chemoreceptor. *J Mol Biol* 426:3642-3655.
3. Lai RZ, Gosink KK, & Parkinson JS (2017) Signaling consequences of structural lesions that alter the stability of chemoreceptor timers of dimers. *J Mol Biol* 429:823-835.
4. Flack CE & Parkinson JS (2018) A zipped-helix cap potentiates HAMP domain control of chemoreceptor signaling. *Proc Natl Acad Sci U S A* 115:E3519-E3528.
5. Ames P, Hunter S, & Parkinson JS (2016) Evidence for a Helix-Clutch Mechanism of Transmembrane Signaling in a Bacterial Chemoreceptor. *J Mol Biol* 428:3776-3788.
6. Kitanovic S, Ames P, & Parkinson JS (2015) A Trigger Residue for Transmembrane Signaling in the Escherichia coli Serine Chemoreceptor. *J Bacteriol* 197:2568-2579.
7. Pinas GE, Frank V, Vaknin A, & Parkinson JS (2016) The source of high signal cooperativity in bacterial chemosensory arrays. *Proc Natl Acad Sci U S A* 113:3335-3340.
8. Piñas GE, DeSantis MD, & Parkinson JS (2018) Noncritical sgnaling role of a knase-receptor iteraction surface in the *Escherichia coli* chemosensory core complex. *J Mol Biol* 430:1051-1064.
9. Ames P, Studdert CA, Reiser RH, & Parkinson JS (2002) Collaborative signaling by mixed chemoreceptor teams in *Escherichia coli*. *Proc Natl Acad Sci U S A* 99:7060-7065.
10. Studdert CA & Parkinson JS (2005) Insights into the organization and dynamics of bacterial chemoreceptor clusters through *in vivo* crosslinking studies. *Proc Natl Acad Sci U S A* 102:15623-15628.
11. Ames P, Zhou Q, & Parkinson JS (2008) Mutational analysis of the connector segment in the HAMP domain of Tsr, the *Escherichia coli* serine chemoreceptor. *J Bacteriol* 190:6676-6685.
12. Zhou Q, Ames P, & Parkinson JS (2011) Biphasic control logic of HAMP domain signalling in the *Escherichia coli* serine chemoreceptor. *Mol Microbiol* 80:596-611.
13. Frank V, Pinas GE, Cohen H, Parkinson JS, & Vaknin A (2016) Networked chemoreceptors benefit bacterial chemotaxis performance. *MBio* 7:01824-01816.